SINGLE ELECTRON TRANSFER CROSS SECTIONS FOR CARBON, NITROGEN, OXYGEN, AND FLUORINE IONS INCIDENT ON HELIUM

by

THOMAS RANDALL DILLINGHAM

B. S., University of Southern Colorado, 1977

A MASTER'S THESIS

submitted in partial fulfillment of the

requirements for the degree

MASTER OF SCIENCE

Department of Physics

KANSAS STATE UNIVERSITY
Manhattan, Kansas

1980

Approved:

Patrick Richard
Major Professor

THIS BOOK
CONTAINS
NUMEROUS PAGES
WITH THE ORIGINAL
PRINTING BEING
SKEWED
DIFFERENTLY FROM
THE TOP OF THE
PAGE TO THE
BOTTOM.

THIS IS AS RECEIVED
FROM THE
CUSTOMER.

Spec. Coll.
LD
2668
.T4
1980
D54
c.2

TABLE OF CONTENTS

LIST OF FIGURES

LIST OF TABLES

ACKNOWLEDGEMENTS

This work is dedicated to the memory of Dr. James R. Macdonald whose enthusiasm for his work and love of life were a continuous source of inspiration for me. His encouragement and guidance enabled me to grow both as a researcher and as a person.

I would like to thank the members of my committee, Dr. Patrick Richard, Dr. James McGuire, and Dr. Basil Curnutte, for their valuable comments and suggestions concerning the contents of this work. Their patience and concern are greatly appreciated.

To my parents, sister, and grandmother goes a very special thanks. One's accomplishments have little meaning without others with whom they can be shared. Thank you all for the love and support you have given me.

I also would like to acknowledge the U.S. Department of Energy, Division of Chemical Sciences, for their financial support during the course of this work.

I. INTRODUCTION

The processes that can occur in an ion-atom collision define a subject which has captivated a great deal of attention over the past years.[1] Renewed interest in understanding these processes stem from their applications to such diverse fields of study as fusion technology[2] and x-ray astronomy.[3] In addition, the subject is of considerable theoretical interest.[4] By utilizing the well-known Coulomb potential and the known initial and final atomic states, one hopes to be able to test the validity of various approximations to collision theory.

There are many commonly identified processes that can take place with varying degrees of probability when an incoming projectile interacts inelastically with a target atom. Some of these include the capture of one or more electrons from the target by the projectile, ionization of the projectile electrons (electron loss), ionization of the target electrons, and excitation of either or both the projectile and target atoms. Often, the reactants are left in excited states following the collision and photons or electrons may be emitted, either independent of the collision or perturbed by it, and observation of these has lead to much of our knowledge of the collision mechanisms.[1] Although all the processes are of current interest, this thesis will be limited to the study of the single electron transfer process in which one electron is either captured or lost by an initial ground state one-electron projectile ion interacting with helium target atoms. The experimental techniques used are similar to those used in previous studies[5,6] of charge exchange by the "initial growth method," performed for various ions over a range of energies. Review of earlier work has been given

by Allison and Garcia-Munoz,[7] Nikolaev,[8] Betz,[9] and Tawara and Russek.[10] Other than for low Z projectiles (H,He) there has been no concerted effort to study these processes for the well-defined initial states of a one-electron ion for which theoretical calculations are presumably possible.

The prime purpose of the present work is to use charge transfer measurements to determine K-shell ionization cross sections which have previously been determined from other types of experiments,[11] for example, x-ray or Auger electron observations. The latter work has focused on ionization of inner-shell electrons from neutral target atoms while the present work is limited to the ionization of hydrogen-like projectile ions in collision with simple atoms i.e. He. The understanding of the process of ionization of neutral atoms by collision with a charged particle are complicated by the presence of other electrons on the atom.[12] For the one-electron ions used in this experiment, the wave functions are purely hydrogenic (unscreened) and no screening parameterization is required for the electron to be ionized.

In most previous experimental work dealing with the ionization process, it has been tacitly assumed that target atoms are ionized by swift, point charge, projectiles. In this work, ionization of the projectile ion is studied. The comparison with other work is straightforward since it is the relative velocity between the projectile and target which defines the collision, and not which atom is the projectile. However, we must examine the role of target electrons which are present on the neutral target atom. The present experimental results must be compared at the same relative velocity, not laboratory energy, to

calculations and other relevant measurements. Cross sections are defined with the relative velocity as an important parameter.

One complication to the interpretation of the present experiment, not present in more traditional work, is the presence of outer shell electrons on the helium target atoms interacting with the projectiles. The consequence of the screening of these electrons has not been well established in the literature and remains a subject for further investigation.[13,14]

II. THEORETICAL FRAMEWORK

a.) Ionization

The excitation and ionization of electrons in an ion-atom collision can be described theoretically by the Plane Wave Born Approximation.[4,15,16] To illustrate the PWBA derivation, with the specific approximations involved, consider the following. The Schröinger equation to be solved is given by

$$\left(\frac{-\hbar^2}{2\mu}\nabla^2 + V\right)\psi = E\psi \tag{2-1a}$$

or

$$(\nabla^2 + k^2)\psi = U\psi \tag{2-1b}$$

where $k^2 = 2\mu E/\hbar^2$ and $U = 2\mu V/\hbar^2$. The solution of this equation can be written in terms of the appropriate Green's function $G(\vec{R},\vec{R}')$[15] and is given by

$$\psi_k(\vec{R}) = \frac{1}{(2\pi)^{3/2}} e^{i\vec{k}\cdot\vec{R}} - \frac{1}{4\pi}\int G(\vec{R},\vec{R}')\, U(\vec{R}')\, \psi_k(\vec{R}')\, d^3R' \tag{2-2}$$

where

$$G(\vec{R},\vec{R}') = \frac{\exp(ik|\vec{R}-\vec{R}'|)}{|\vec{R}-\vec{R}'|} \quad . \tag{2-3}$$

For large R, the solution can be approximated by

$$\psi_k(\vec{R}) \approx \frac{1}{(2\pi)^{3/2}} e^{i\vec{k}\cdot\vec{R}} - \frac{e^{ikR}}{4\pi R}\int e^{-i\vec{k}'\cdot\vec{R}'}\, U(\vec{R}')\, \psi_k(\vec{R}')\, d^3R' \tag{2-4}$$

where $\vec{k}$ is the beam direction and $\vec{k}' = k'\hat{R}$. This assymptotic form can be re-written as

$$\psi_k \approx \frac{1}{(2\pi)^{3/2}} \left(e^{i\vec{k}\cdot\vec{R}} + \frac{e^{ikR}}{R} f_k\right) \tag{2-5}$$

where f_k, the scattering amplitude, is given by

$$f_k = -\frac{(2\pi)^{3/2}}{4\pi} \int e^{-i\vec{k}'\cdot\vec{R}'} U(\vec{R}') \psi_k(\vec{R}') \, d^3R'. \tag{2-6}$$

Now, the differential cross section for a particle scattered by the potential V can be written in terms of the scattering amplitude as

$$\frac{d\sigma}{d\Omega} = |f_k|^2 \tag{2-7}$$

corresponding to the intensity of the outgoing wave. In the first Born approximation, the exact eigenfunction $\psi_k(\vec{R}')$ in Eq. (2-6) is replaced by a plane wave, and the deviation of the scattered wave from a plane wave considered negligable. With this approximation, the scattering amplitude becomes

$$f_k \approx -\frac{\mu}{2\pi\hbar^2} \int e^{-i\vec{k}'\cdot\vec{R}'} V(\vec{R}') \, e^{i\vec{k}\cdot\vec{R}'} \, dR' \tag{2-8}$$

and is proportional to the matrix element of the scattering potential between two plane waves $e^{i\vec{k}\cdot\vec{R}'}$ and $e^{-i\vec{k}'\cdot\vec{R}'}$, which represent the free particle before and after the interaction respectively.

To use the PWBA expression for excitation or ionization of electrons in a hydrogen-like system, the wave functions are replaced by a hydrogen-like wave function, $\phi_i(\vec{r})$, times a plane wave. Thus the scattering amplitude becomes

$$f(q) = \frac{-\mu}{2\pi\hbar^2} \int \phi_f^*(\vec{r})\ V\ \phi_i(\vec{r})\ e^{i\vec{q}\cdot\vec{R}}\ d\vec{r}\ d\vec{R} \qquad (2\text{-}9)$$

where q is the momentum transferred in the collision, $q = |\vec{k}-\vec{k}'|$, and $\vec{r}$ and $\vec{R}$ are now the electronic and internuclear coordinates as shown in Figure 1. The PWBA cross section for ionization of a hydrogen-like ion can be written in terms of a universal function[17] scaled by a factor which is dependent only upon the atomic numbers, Z_1 and Z_2, of the projectile and target atoms respectively. To show the scaling with Z_1 and Z_2,[13,16] the total cross section, σ, for excitation or ionization can be written in terms of the scattering amplitude as

$$\sigma = \frac{1}{\mu^2 v^2} \int_{q_{min}}^{q_{max}} |f(q)|^2\ q\,dq \qquad (2\text{-}10)$$

where v is the relative velocity, and where atomic units ($\hbar = e = 1$) have been used. q_{min} is the minimum momentum transfer in the collision and is given by

$$q_{min} = k - k'_{max} \approx \frac{\Delta E}{2v}\left(1 + \frac{\Delta E}{2\mu v^2}\right) \approx \frac{\Delta E}{2v} \qquad (2\text{-}11)$$

where $k'^2_{max} = 2\mu(E - \Delta E)$, ΔE being the threshold energy of the process. The approximations for q_{min} are valid for $\frac{\Delta E}{E} << 1$. Since $\Delta E \sim Z_2^2$, the minimum momentum transfer can be written as

$$q_{min} \approx \frac{Z_2^2}{2v} \quad . \qquad (2\text{-}12)$$

Figure 1 Diagram showing the electronic coordinate $\vec{r}$, and the internuclear coordinate $\vec{R}$.

THIS BOOK CONTAINS NUMEROUS PAGES WITH DIAGRAMS THAT ARE CROOKED COMPARED TO THE REST OF THE INFORMATION ON THE PAGE.

THIS IS AS RECEIVED FROM CUSTOMER.

Figure 1

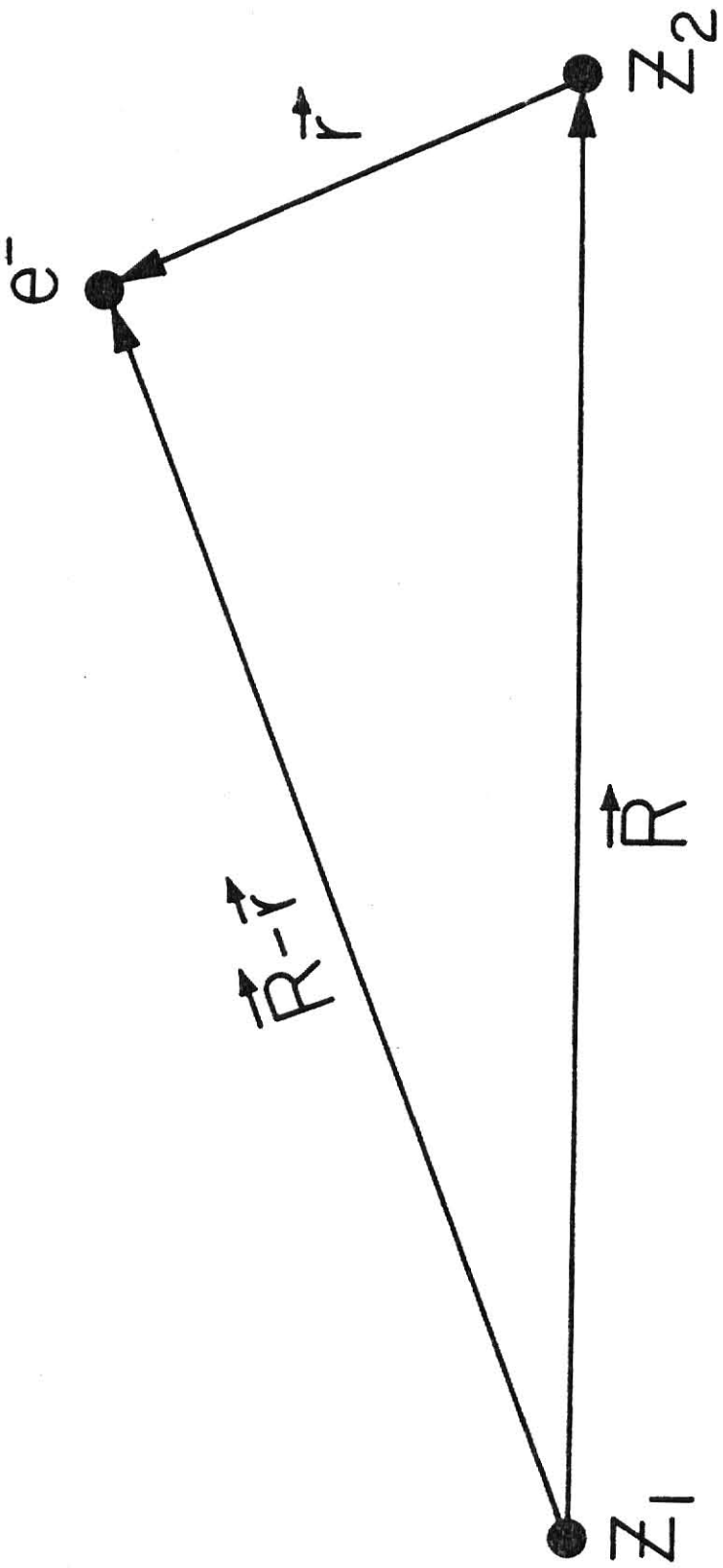

The maximum momentum transfer, q_{max} is given by

$$q_{max} = k + k'_{max} \approx 2k \tag{2-13}$$

which is large enough to be taken as infinite for mathematical convenience. Thus, the total cross section in the PWBA can be written as

$$\sigma = \frac{1}{\mu v^2} \int_{Z_2^2/2v}^{\infty} |f(q)|^2 \, q dq \tag{2-14}$$

where the scattering amplitude, using the Coulomb potential between the projectile and the electron of interest, is given by

$$f(q) = \frac{-\mu}{2\pi} \int \phi_i(\vec{r}) \quad \frac{Z_1}{|\vec{r} - \vec{R}|} \quad \phi_f(\vec{r}) e^{i\vec{q}\cdot\vec{R}} \, d\vec{r} d\vec{R} \quad . \tag{2-15}$$

For hydrogen-like ions with different atomic number, Z_2, the scaling of the coordinates for hydrogen-like wave functions is given by

$$\begin{aligned} r &\rightarrow \rho/Z_2 & d\vec{r} &= d\vec{\rho}/Z_2^3 \\ R &\rightarrow \hbar/Z_2 & d\vec{R} &= d\vec{\hbar}/Z_2^3 \end{aligned} \tag{2-16}$$

$$\& \quad \phi(\vec{r}) = Z_2^{3/2} \, \phi(\vec{\rho})$$

so,

$$f(q) = \frac{-\mu}{2\pi} \int Z_2^{3/2} \, \phi_i(\rho) \, \frac{Z_1 Z_2}{|\vec{\rho} - \vec{\hbar}|} \, Z_2^{3/2} \, \phi_f(\rho) e^{i\vec{q}\cdot\vec{\hbar}/Z_2} \, \frac{d\vec{\rho}}{Z_2^3} \frac{d\vec{\hbar}}{Z_2^3} \, . \tag{2-17}$$

From this scattering amplitude, the cross section is given by eq. (2-14)

$$\sigma = \frac{Z_1^2}{Z_2^4} \int_{Z_2^2/2v}^{\infty} \left[\frac{\tilde{f}(\frac{q}{Z_2})}{\mu}\right]^2 \frac{q}{v}\frac{dq}{v} \tag{2-18}$$

letting $Q = q/Z_2$ and $V = \frac{v}{Z_2}$ (2-19)

$$\sigma = \frac{Z_1^2}{Z_2^4}\frac{1}{V^2} \int_{1/2V}^{\infty} \left[\frac{\tilde{f}(Q)}{\mu}\right]^2 QdQ \tag{2-20}$$

$$\sigma = \frac{Z_1^2}{Z_2^4}\frac{F(V)}{V^2} = \frac{Z_1^2}{Z_2^4} F'(V) \quad . \tag{2-21}$$

So the excitation or ionization cross section can be written in terms of a function $F'(V)$, scaled by the factor Z_1^2/Z_2^4. V, in atomic units, is the scaled velocity for a one-electron ion with nuclear charge Z_2.

Ionization cross sections were computed by the PWBA method for protons on hydrogen.[18,19] Appendix 1 lists the function $F'(V)$, giving the cross section as a function of projectile velocity. To obtain the cross sections for other systems, the scaling law gives

$$\sigma(Z_1, Z_2, v_{inc}) = \frac{Z_1^2}{Z_2^4}\sigma(1, 1, v_{inc}/Z_2) \tag{2-22}$$

where v_{inc} is the relative velocity between the projectile and target atoms. An example of the scaling for O^{+7} on He is given in the Appendix.

It should be noted that the He atom is treated as a pure point charge. The effects of screening by the He electrons are not included in this calculation.

Other studies in the literature[20,21] utilize the PWBA in the range where $Z_1/Z_2 < 1$. In these works, a screening parameter, θ_K, is used to account for the departure from hydrogen-like wave functions. In this thesis, screening parameters are not needed for the projectile since the incident ions are in pure hydrogen-like states. θ_k in this case, equals 1. Also included in these works are Coulomb deflection and binding energy corrections. These corrections, incorporated in an approximate manner, account for the deflection of the projectile by the target nucleus, and the pertubation, by the projectile, of the atomic states of the target atom. The contribution to the PWBA ionization cross sections by these correction terms, are shown later in this thesis.

b.) Electron Capture; Comparison with X-ray Cross Sections.

The process in which a target electron is captured by the projectile is also of interest in this study. With the experimental methods used in this work, measurements of the total cross sections for both the ionization and capture processes are obtained simultaneously.

When an electron is captured by the projectile ion, an x-ray may be emitted after the collision in a de-excitation process, provided the electron was captured to an excited state of the projectile. The x-ray and capture cross sections can be related through a function $g(Z_1, E)$ according to Guffey,[22] where

$$g(Z_1, E) = \left[\frac{\sigma_{2p}}{\sigma_{TC}}\right]_{(Z_1, E)} + [1 - 0.12\ B(Z_1)] \cdot \sum_{n=3,\ell}^{n_{max}} \left[\frac{\sigma_{n\ell}}{\sigma_{TC}}\right]_{(Z_1, E)} . \qquad (2\text{-}23)$$

The function essentially represents the fraction of capture events that give rise to K x-rays and can be calculated if the capture cross section to each state is known. The factor $0.12\ B(Z_1)$ represents the branching ratios for the states produced in capture to the Z_1 nucleus such that a K x-ray occurs in the decay process. Guffey evaluated the capture cross sections, $\sigma_{n\ell}$, through a Brinkman-Kramers formulation and related the results to the x-ray cross sections by means of

$$\sigma_x\ (Z_1,E) = \overline{N}\ g(Z_1,E) \cdot \sigma_{TC}(Z_1,E) \qquad (2\text{-}24)$$

where $\overline{N}$ is the overall normalization constant. The normalization constant was included since it is well known that the B-K approximation leads to a large over-estimation of the cross section. More recent theoretical work for other systems[23] have improved on the OBK approximation in giving the absolute capture cross section, but for capture of loosely bound electrons, such calculations have not yet been published. From the total capture cross sections found in this work, and the x-ray cross sections from Guffey, the value of $g(Z_1,E)$ was calculated and compared to the value found through the Brinkman-Kramers formulation. The results of this comparison will be given later in the text.

III. ELECTRON TRANSFER EXPERIMENTS

a.) Definition of Process

When a beam of projectile ions of a given charge state is incident on a target, a fraction of the beam undergoes charge exchange with the target atoms. Thus, the outgoing beam contains ions with a variety of different charge states. These charge states can be expressed in terms of the relative charge fractions, ϕ_i, where ϕ_i is the ratio of the number of ions in state i to the total number of ions in all states, and is given by

$$\phi_i = \frac{n_i}{\sum_i n_i} \tag{3-1}$$

where n_i is the number of ions in a given state i. Since an ion may also be excited by the target, a charge fraction measurement represents a summation over the excited states for each ionic charge emerging from the target. Any excited state that decays by a mechanism that changes the charge of an ion (Auger emission, for example) will be included in the summation for the final charge state.

In general, the change in charge state of a beam of ions as it passes through a target is given by the following set of differential equations.[24]

$$\frac{d\phi_i}{dx} = \sum_{j \neq i} (\sigma_{ji}\phi_j - \sigma_{ij}\phi_i) \tag{3-2}$$

where x is the target thickness in atoms/cm^2. The equations are written in terms of the charge exchange cross sections, σ_{ij}, of an ion changing from a charge state i to a state j after undergoing a collision with a target atom. Total charge transfer cross sections are summations over cross sections for formation of well-defined atomic states and in general depend upon many factors including the possible distribution of final states of both projectile and target. However, attempts have been made to identify the dependence of the total charge transfer cross sections on the relative velocity between the projectile and target, the charge state and atomic number of the ions, and the state of excitation of the incoming beam. Dependence upon the latter can be removed by choosing a long flight path of the incident beam before it reaches the target chamber, such that the time of flight is longer than the lifetimes of the excited states. For example, the flight time for 1 MeV/amu ions from the foil stripper to the target chamber in the present experiment is approximately 10^{-6} sec. This is long compared to the lifetimes[25] of the states of the ions of this experiment with the exception of the helium-like $(1s2s)\,^3S_1$ state and the hydrogen-like 2s state. These lifetimes, plus others of interest, are listed in Table (3-1) for the ions used in this experiment. For the hydrogen-like state, the excited state is quenched in the motional electric field of the charge selection magnet, while the helium-like state will survive to the target chamber.

Table 3-1 A summary of the lifetimes for the various excited states of the ions used in this experiment.

Table 3-1

	State	Z	Lifetime (sec.)
Hydrogen-like	(2s)	6	2.60×10^{-6}
		7	1.03×10^{-6}
		8	4.64×10^{-7}
		9	2.29×10^{-7}
	(2p)	6	1.64×10^{-12}
		7	8.86×10^{-13}
		8	5.20×10^{-13}
		9	3.24×10^{-13}
	(3p)	6	1.38×10^{-11}
		7	7.47×10^{-12}
		8	4.38×10^{-12}
		9	2.73×10^{-12}
Helium-like	$(1s2s)\,^1S_0$	6	3.02×10^{-6}
		7	1.06×10^{-6}
		8	4.33×10^{-7}
		9	1.98×10^{-7}
	$(1s2s)\,^3S_1$	6	2.06×10^{-2}
		7	3.95×10^{-3}
		8	9.62×10^{-4}
		9	3.27×10^{-4}
	$(1s2p)\,^1P_1$	6	1.13×10^{-12}
		7	5.54×10^{-13}
		8	3.03×10^{-13}
		9	1.79×10^{-13}

	$(1s2p)^3P_0$	6	1.77×10^{-8}
		7	1.47×10^{-8}
		8	1.26×10^{-8}
		9	1.10×10^{-8}
	$(1s2p)^3P_1$	6	1.18×10^{-8}
		7	4.8×10^{-9}
		8	1.6×10^{-9}
		9	5.2×10^{-10}
	$(1s2p)^3P_2$	6	1.75×10^{-8}
		7	1.44×10^{-8}
		8	1.22×10^{-8}
		9	1.04×10^{-8}
Lithium-like	$(1s2s2p)^4P_{1/2}$	6	1.60×10^{-7}
		7	3.68×10^{-8}
		8	1.07×10^{-8}
		9	3.57×10^{-9}
	$(1s2s2p)^4P_{3/2}$	6	6.37×10^{-8}
		7	1.45×10^{-8}
		8	4.20×10^{-9}
		9	1.39×10^{-9}
	$(1s2s2p)^4P_{5/2}$	6	8.85×10^{-8}
		7	4.27×10^{-8}
		8	2.30×10^{-8}
		9	1.28×10^{-8}

b.) Apparatus

Negative ions, extracted from the diode ion source, were accelerated in the KSU tandem Van de Graaff accelerator. To produce the desired ions, a second gas line was used to inject another gas into the hydrogen arc. To obtain a carbon or nitrogen beam, a mixture of nitrogen and methane gas was introduced into the source. This mixture produces CN^- ions for acceleration. OH^- ions, obtained from water vapor, were used to produce an oxygen beam. Negative F ions are usually available as a contaminant in the ion source. However, when a sufficient beam current could not be obtained, sulfur hexafluoride, SF_6, was injected into the source to produce a fluorine beam.

The negative ions were accelerated to the high voltage terminal of the accelerator, see Figure 2. By using either a gas or a foil stripper, electrons of the negative ions are stripped off at the terminal. The positive ions that are produced are accelerated away from the terminal with different energies depending upon the charge state of the ion. A 90^o analyzing magnet was then used to momentum analyze the ions and select out those with the desired energy. To produce different charge states, the beam was passed through a thin carbon foil ($5-20\mu g/cm^2$) after the analyzing magnet. The charge state of interest was then selected by a switching magnet which directs the beam down the beam line to the target chamber. This technique provides ions of a range of charge states at the same beam energy.

The target chamber consisted of a differentially pumped gas cell as shown in Figure 3. The overall length of the gas cell was 19.61 cm, and was defined by four optically aligned circular apertures. The size of

Figure 2 A schematic diagram of the Kansas State University tandem Van de Graaff accelerator.

Figure 2

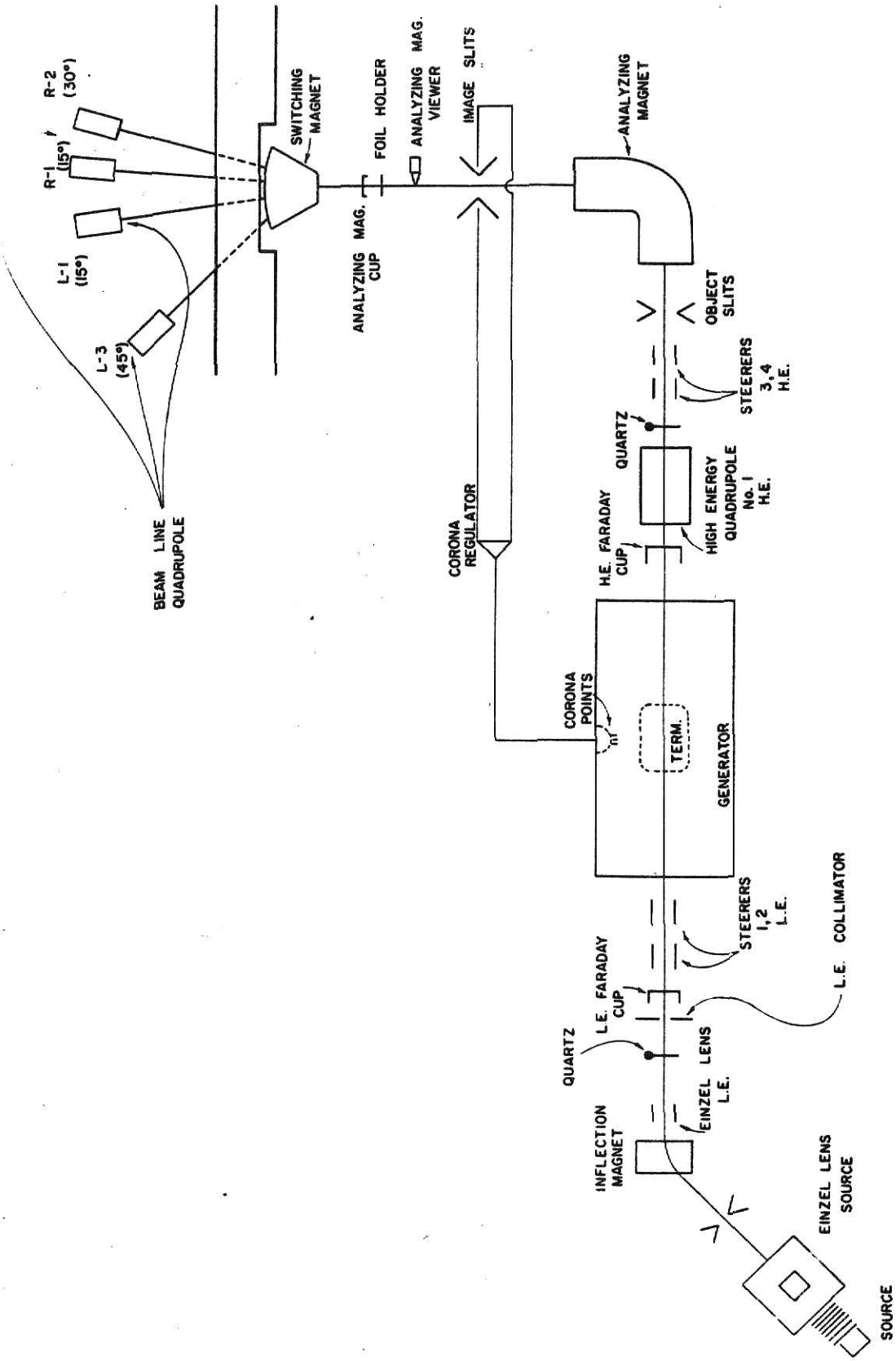
R-2 (30°)
R-1 (15°)
L-1 (15°)
L-3 (45°)
BEAM LINE QUADRUPOLE
SWITCHING MAGNET
ANALYZING MAG. CUP
FOIL HOLDER
ANALYZING MAG. VIEWER
IMAGE SLITS
CORONA REGULATOR
ANALYZING MAGNET
OBJECT SLITS
STEERERS 3,4 H.E.
QUARTZ
HIGH ENERGY QUADRUPOLE No. 1 H.E.
H.E. FARADAY CUP
CORONA POINTS
TERM.
GENERATOR
STEERERS 1,2 L.E.
L.E. COLLIMATOR
L.E. FARADAY CUP
QUARTZ
EINZEL LENS L.E.
INFLECTION MAGNET
EINZEL LENS SOURCE
SOURCE

Figure 3 A schematic diagram of the gas target chamber and charge spectrometer with position sensitive detector.

Figure 3

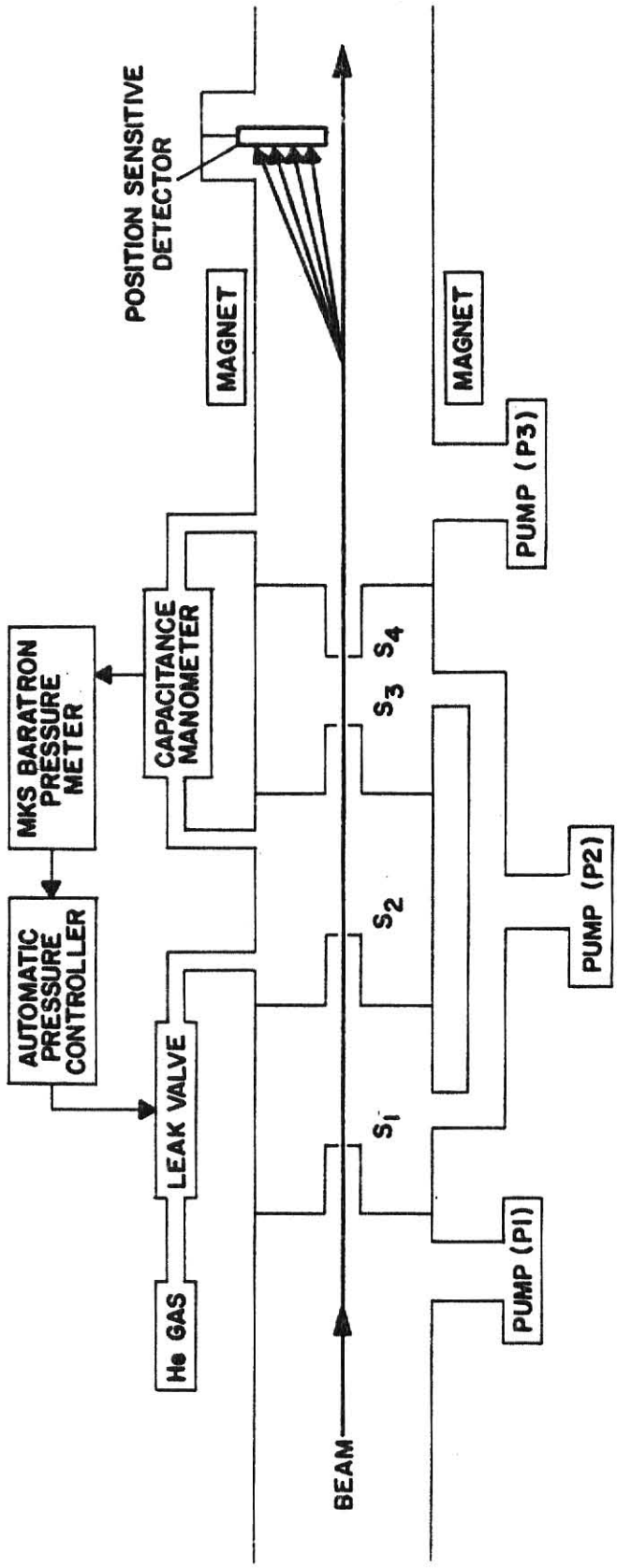
POSITION SENSITIVE DETECTOR
MAGNET
MAGNET
PUMP (P3)
MKS BARATRON PRESSURE METER
CAPACITANCE MANOMETER
S4
S3
AUTOMATIC PRESSURE CONTROLLER
S2
PUMP (P2)
LEAK VALVE
S1
He GAS
PUMP (P1)
BEAM

the apertures were 1.43, 1.48, 2.41, and 3.01 mm for S1, S2, S3, and S4 respectively. The pumping of the cell was accomplished by means of a 4 inch diffusion pump (P2) connected directly in front of and behind the gas cell. Two other diffusion pumps (P1 and P3) were also utilized to maintain a residual gas pressure of 10^{-6} to 10^{-7} torr in the beam line.

Maintaining a constant pressure within the target chamber was accomplished by means of a Granville-Phillips automatic pressure controller.[26] The pressure was monitored by an MKS Baratron capacitance manometer[27] which sent a signal to the pressure controller (to open or close a valve to the chamber) whenever the pressure deviated from a preset value. To prevent contaminants in the He gas handling system from entering the target chamber, a liquid nitrogen trap was placed in the gas line to extract any condensable vapor contaminants within the system.

As the beam passes through the gas cell, a fraction of the incident particles undergo charge exchange with the target gas. At approximately 80 cm behind the target cell, an electromagnet was set up to spacially separate the various charge states of the emerging beam. After separating the charge states, a position-sensitive surface barrier detector was used to detect the ions of the emerging beam.

The detector, supplied by Nuclear Diodes, was a silicon surface barrier detector capable of providing information about both the energy and position of the incident ion simultaneously. When an ion enters the detector, two signals are produced. The first is the collection of all the negative charge to a low resistance gold layer on the front of the detector and gives a signal proportional to the total energy of the

incident particle. The second is from the collection of a portion of the positive charge collected on a resistive strip in the back of the detector. This signal is the product of the energy of the particle times the fraction of the length from the grounded end of the resistive layer and hence represents the position on which the ion impacted. Since the various charge states are spacially separated by the electromagnet, the position sensitive detector was used to determine the relative number of ions in a given state of the emerging beam.

The supporting electronics for the detector system is shown in Figure 4. The energy and position signals are amplified by two Ortec 109A preamplifiers and two Ortec model 451 spectroscopy amplifiers. After being delayed, the position signal was sent to an ADC and multichannel analyzer. Gating of the ADC was done by the energy signal output from a single channel analyzer. Background particles, arising from such things as slit-edge scattering, which have different energy but the same magnetic rigidity as the particles of interest, are prevented from being counted in the spectrum by the gating process. A typical spectrum is shown in Figure 5 for 25 MeV $O^{+7} \rightarrow$ He at a pressure of 82.4 microns.

c.) Procedure

To perform this experiment, the counting rate of the detector was kept below 1000 cts/sec to prevent electronic pile-up in the system and also to ensure a reasonable lifetime of the detector. The counting rate was monitored by both a scaler and a ratemeter. In a typical run, 4×10^4 and 1×10^5 counts were taken for the incident bare nucleus and

Figure 4 A schematic diagram showing the supporting electronics for the detection system.

Figure 4

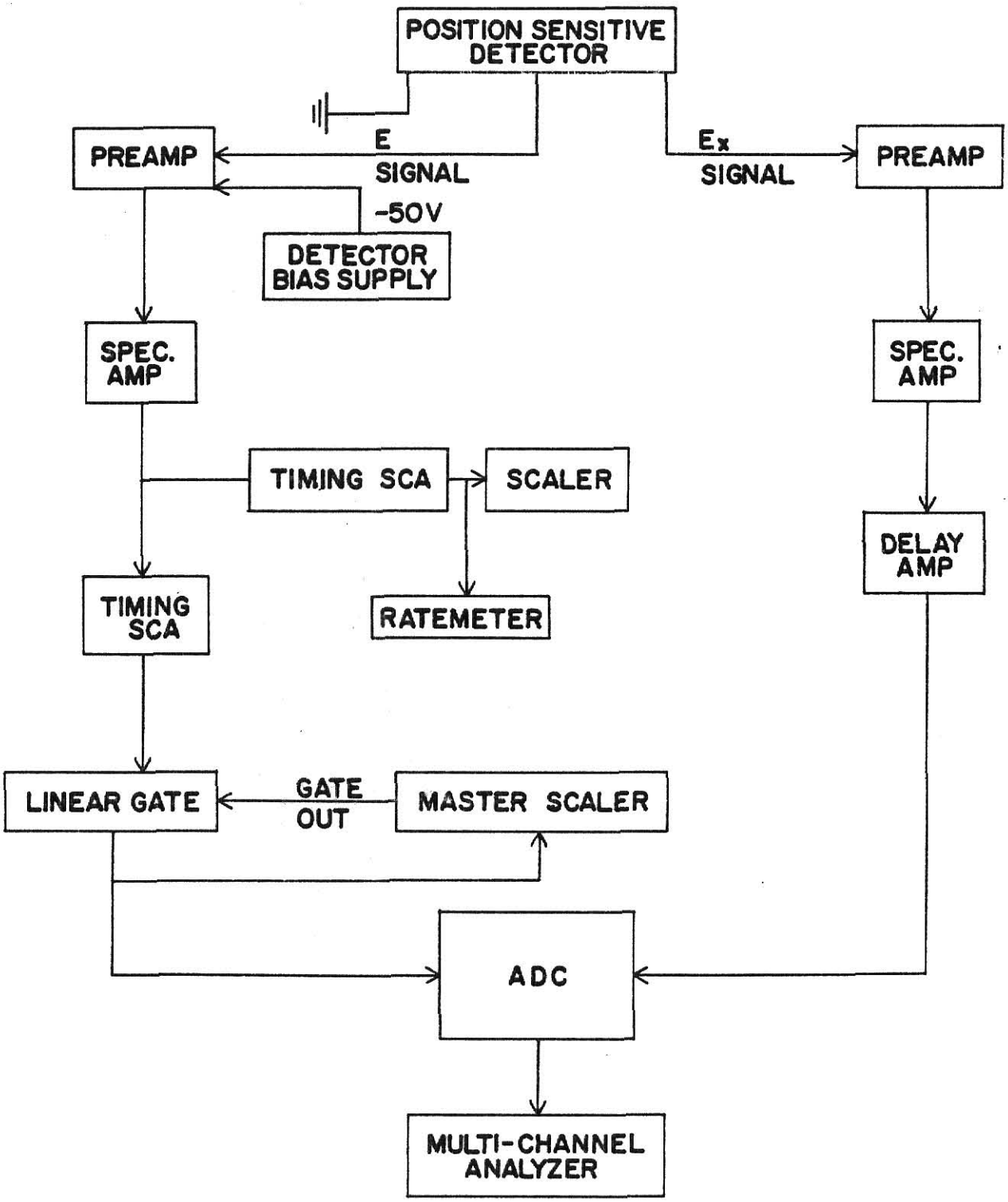
POSITION SENSITIVE DETECTOR
PREAMP
E SIGNAL
-50V
DETECTOR BIAS SUPPLY
Ex SIGNAL
PREAMP
SPEC. AMP
TIMING SCA
SCALER
RATEMETER
TIMING SCA
SPEC. AMP
DELAY AMP
LINEAR GATE
GATE OUT
MASTER SCALER
ADC
MULTI-CHANNEL ANALYZER

Figure 5 A typical position spectrum from the experiment for 25 MeV O^{+7} → He at a pressure of 82.4μ. The spectrum shows the single electron transfer from the +7 to the +6 and +8 charge states for the incident ion.

Figure 5

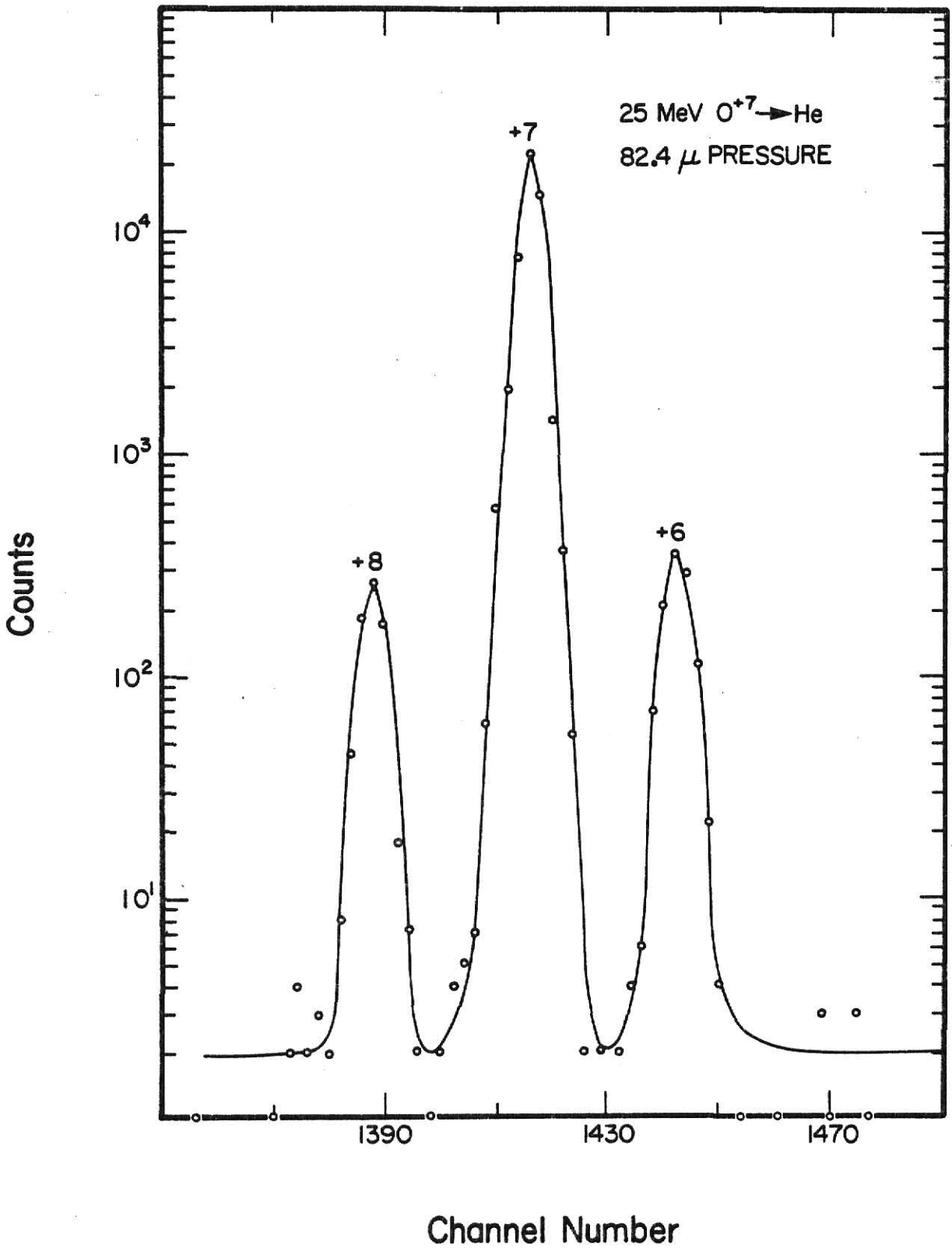
25 MeV O+7 → He
82.4 μ PRESSURE
+7
+8
+6
10^4
10^3
10^2
10^1
Counts
1390
1430
1470
Channel Number

one-electron ions respectively, at a given gas pressure. For each energy, data for at least four different gas pressures were taken.

The pressures were chosen judiciously to ensure "single collision conditions" for the charge exchange process. For this particular work, the criterion for "single collision conditions" was that $\sigma N\ell < 0.1$, where σ is the largest cross section for removing an ion from the incident charge state, N is the number of target atoms per cm^3, and ℓ is the target gas cell length in cm. For this particular experiment, it was found that this criterion permitted a first order solution of Eq. (3-2) to be used to analyze the cross sections. The corrections to the first order approximation of the cross section, and hence the multiple processes, were calculated and in all cases found to be small. Generally, the incident charge state was greater than 95% after undergoing charge exchange. The spectra were analyzed by integrating the number of counts in each peak and calculating the fraction of ions emerging in each charge state at the pressure of the run. The relative charge fractions were then plotted as a function of pressure to obtain the raw data from which the cross sections were determined. As an example of the raw data collected in this experiment, Figure 6 shows the charge fractions, ϕ_i, versus the pressure for 16 MeV $O^{+7} \rightarrow$ He.

d.) Analysis

As a beam passes through a given target, the rate equation for a charge state ϕ_i is given by equation (3-2). A solution to this equation for ϕ_i can be written as

Figure 6 A typical diagram showing the various charge fractions ϕ_i, versus the target cell pressure in microns, for 16 MeV $O^{+7} \rightarrow$ He.

Figure 6

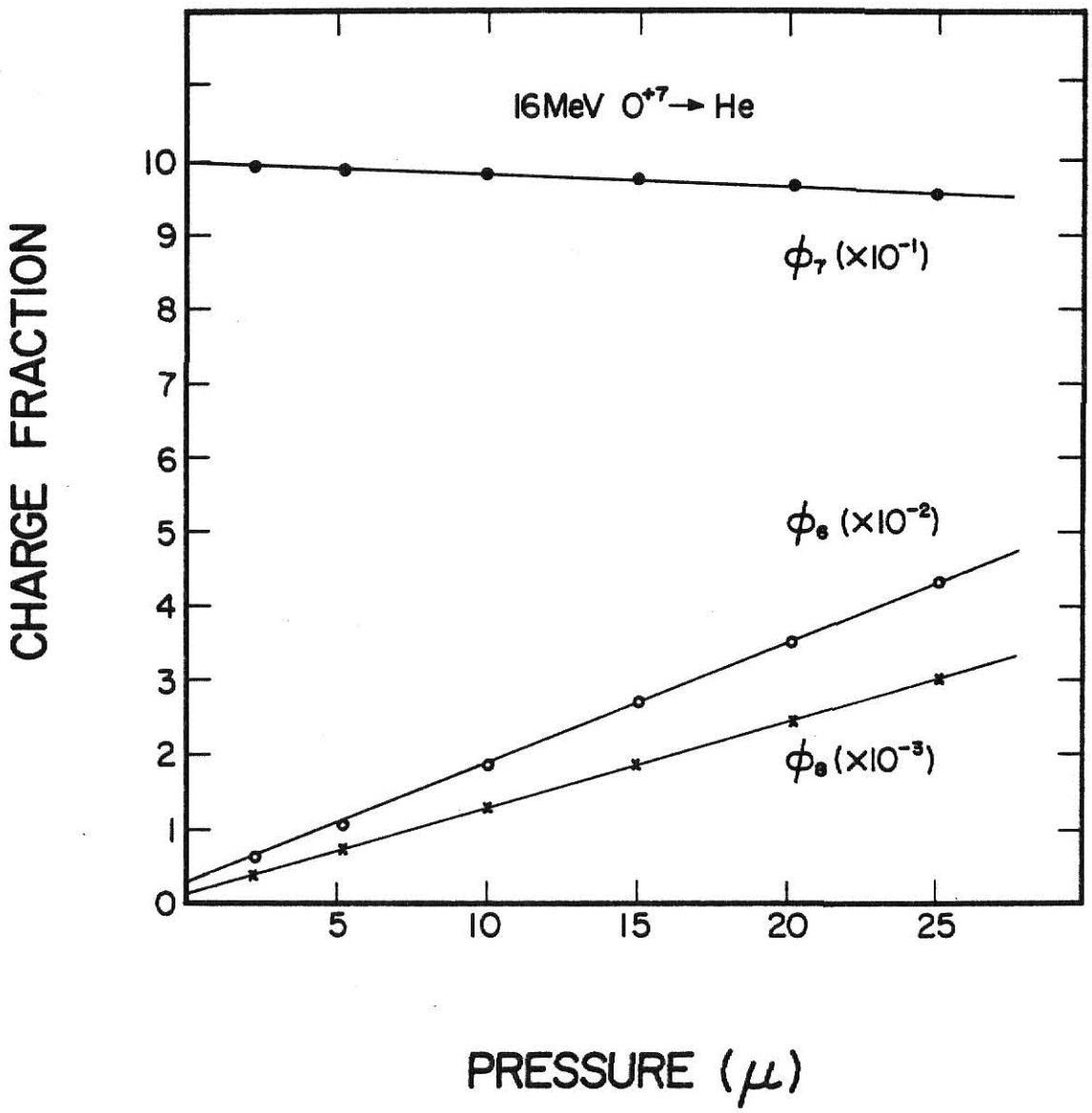
16MeV O+7 → He
CHARGE FRACTION
PRESSURE (μ)
φ7 (×10-1)
φ6 (×10-2)
φ8 (×10-3)
0
1
2
3
4
5
6
7
8
9
10
5
10
15
20
25

$$\phi_i = \phi_i(0) + \sum_{j\neq i} \sigma_{ji}\, x + \sum_{j\neq k}\sum_{k\neq i} \sigma_{jk}\,\sigma_{ki}\, x^2 + \ldots \qquad (3\text{-}3)$$

where an exact solution contains all higher order terms. As a first approximation, one neglects terms other than first order in target thickness x, and the solution becomes

$$\phi_i = \phi_i(0) + \sum_{j\neq i} \sigma_{ji} x \qquad (3\text{-}4)$$

with the initial condition $\phi_\alpha(0) \approx 1$, where α is the incident charge state, and $\phi_{i\neq\alpha}(0) << 1$. Ignoring multiple processes, the single electron transfer cross section can be written as

$$\sigma_{\alpha i} = \frac{d\phi_i}{dx} \qquad (3\text{-}5)$$

Thus the slope of the charge fraction ϕ_i versus the target thickness x, gives a first order approximation to the single electron capture and loss cross sections.

To evaluate the contribution of second order terms to the cross section, we consider only a three state system αij. For a Helium target this is sufficient since double electron transfer cross sections are small. The second order expression is then given approximately by

$$\phi_i \approx \phi_i(0) + \sigma_{\alpha i}\, x(1 \pm \sigma_{\alpha j} x)\, \exp(-\sigma_{\alpha j} x) \qquad (3\text{-}6)$$

$$\phi_i \approx \phi_i(0) + \sigma_{\alpha i}\, x(1 \pm \frac{d\phi_j}{dx} x)\, \exp(-\frac{d\phi_j}{dx} x) \qquad (3\text{-}7)$$

where the sign in the parenthesis is determined by the competing processes which can either add to or subtract from the charge fraction of interest ϕ_i. Also included is an exponential term which accounts for the depletion of the initial charge fraction with target thickness. Thus the corrections to the first-order approximation can be determined from the quantity in parenthesis in Eq. (3-7). In general, the second-order corrections were small, usually less than 3%, although in a few instances, the corrections reached 13%. Even this correction justifies the analysis using the first-order approximations to determine the cross sections.

The target thickness, x in atoms/cm^2, was related to the pressure by means of the ideal gas law in the following equation

$$x = \frac{N_a}{RT} \ell(\text{cm})\ P(\mu) \tag{3-8}$$

where $N_a = 6.025 \times 10^{23}$ atoms/mole (Avagadro's number), R = 8.313 joules/mole - ^oK (universal gas constant), T is the temperature in units of ^oK, ℓ is the target cell length in cm, and P is the pressure in units of microns of Hg. Using this, the single charge transfer cross section can be written as

$$\sigma_{\alpha i} = k \frac{d\phi_i}{dP(\mu)} \tag{3-9}$$

where $k = RT/N_a\ell$ is a constant. T is assumed to be room temperature throughout the course of the experiment. The value of k can be found

by precisely measuring the target length ℓ. The absolute scale calibration, determined in this way, was also checked by a normalization process discussed later in this work.

To obtain the experimental cross sections, the values of $d\phi_i/dP(\mu)$ were determined for each charge fraction ϕ_i. A program was developed to obtain the best straight line fit to the experimental data points by a least squares method.[27] The slope of this line, along with the constant k, was used to find the single charge transfer cross sections to first-order. This value was then improved by incorporating the second-order correction term given previously. This procedure was performed for each ion to obtain the single charge transfer cross sections over the energy range of interest.

e.) Errors and Uncertainties

The uncertainty in a quantity measured experimentally is dependent upon the precision of the instruments used and the propagation of these errors in the analysis. In this work, there are two major sources that contribute to the uncertainty in the measurements. These include the uncertainty in the measured gas pressure within the target chamber, and the statistical error arising from the number of counts in each peak in a spectrum, where each peak corresponds to a given charge state. Other sources of error in the absolute cross section include the absolute pressure calibration, the efficiency of detecting a charged particle at a given position along the position-sensitive detector, and the uncertainty in determining the absolute normalization constant k.

To eliminate the uncertainty in detector efficiency over the range of the detector, different magnet settings and detector positions were used throughout the course of the experiment. Periodically, the spectra were checked while changing the magnet current or detector position to ensure the best possible resolution and also to see that the efficiency of the different positions along the detector was not changing.

In most spectra, the peak to background ratio is large enough that background particles being counted do not play a significant role in adding to the uncertainty of the charge transfer measurements. In a few instances, where the cross section is small, and that to other states large did this factor introduce any significant error into the measurements. Even in these cases other errors were larger than this contribution and it was not included in the calculation of the error in the cross sections.

To minimize the error in the pressure reading, the pressure was measured both at the start and finish of a run. The average of these two values was taken as the pressure within the target chamber. Any run where the difference in pressure from start to finish varied by more than 10% of the full scale value was deleted and the data retaken. Usually the cell pressure was at least equal to the full scale manometer setting. In general, the pressure drift was less than 3% of the full scale value from start to finish, while the quoted accuracy of the pressure meter is from 1 - 3% of the full scale value. Utilizing the instrumental error, the relative error in the pressure reading was obtained by multiplying this value times the full scale value. The percent error was then found by comparing this to an intermediate pressure of a given run.

To find the total error on the cross section, other contributions must also be considered. In the least squares fitting program, the uncertainty in the slope for the best straight line fit was calculated. The error in the slope was compared to the statistical error inherent in the number of counts at an intermediate pressure. The larger of these two values was added in quadrature to the pressure error to give the total relative error for a given first-order cross section. In general, the relative errors on the charge transfer cross sections are less than 10%.

Since the absolute normalization of the cross sections comes from the constant k in Eq. (3-9), the choice of the constant used could introduce a systematic error in all the measurements, thereby effecting the absolute error. Several different methods were used to check and recheck the value of this constant. All of the values obtained for k, utilizing the different methods, agree within the experimental error. The uncertainty in k, and hence the error due to the absolute normalization of the cross sections, is less than 6%. The methods used to evaluate this constant will be discussed in the following section.

f.) Normalization

The first method of evaluating k is through geometric considerations. The relationship between the target thickness and the pressure in the gas cell is given by Eq. (3-8). The constant k is then simply a function of the target cell parameters, $k = RT/N_a\ell$. Care was taken in evaluating the cell length since cell end effects could play a role. The cell length used in this evaluation was the measured cell length plus three

times the radius of the slits at the front and back of the cell.[28] The correction to the length of the cell was approximately 3%. The value of k measured in this fashion was found to be $k = 1.55 \times 10^{-15} \pm .09$ cm^2 $-\mu$/atom.

This value was checked by comparison with other experimental measurements,[5,6] which together give the charge transfer cross sections for C, N, O, and F in argon gas. With the experimental set-up and procedure used in this work, the experiments in argon were redone to obtain values for the change in the charge fraction versus pressure, $d\phi_i/dP(\mu)$. The normalization constant was then obtained by using the cross sections from the previous measurements in argon. This was done using different ions with different energies and the results were compared to the value of k found through geometric considerations. Table 3-2 lists the values of k found by the various methods. The average of these values agree to within 6%.

An approximate normalization to experimental results is available for the electron capture cross sections using the total x-ray cross sections for fluorine on He by Guffey.[22] The x-ray cross sections provide a lower limit to the total electron capture cross sections, and were used to determine a lower limit to the normalization constant. The value of the constant obtained was approximately 80% of that found geometrically. One would expect this difference since a K x-ray is emitted when the electron is captured to a state other than the 1s and 2s states and then only with a branching ratio that is approximately 88%.[22] Hence the total x-ray cross section is less than the total capture cross section and the results of this comparison confirm the

Table 3-2 A summary of the values found for the normalization constant k. The values of k were found through geometric considerations, using previously measured charge transfer cross sections in argon, and previous x-ray measurements. The values from the x-ray measurements provide a lower limit to the normalization constant.

Table 3-2

	Normalization Constant -k
Geometrically	1.55×10^{-15} cm^2 -μ/atom
23.5 MeV O^{+8} → Ar	1.22×10^{-15}
25.0 MeV F^{+9} → Ar	1.62×10^{-15}
18.25 MeV N^{+6} → Ar	1.42×10^{-15}
18.25 MeV N^{+7} → Ar	1.55×10^{-15}
17.85 MeV C^{+6} → Ar	1.45×10^{-15}
17.85 MeV C^{+5} → Ar	1.42×10^{-15}
17.85 MeV C^{+6} → Ar	1.62×10^{-15}
	Ave: 1.47×10^{-15}
From x-ray Measurements (lower limit)	
19 MeV F^{+9} → He	1.27×10^{-15}
32 MeV F^{+9} → He	1.09×10^{-15}

magnitude of the x-ray cross sections to an accuracy of approximately 30%.

For the normalization of the final data, the value used for the normalization constant k was the value found utilizing geometric considerations ($k = 1.55 \times 10^{-15} \pm .09$ cm^2-μ/atom). The other methods used, namely comparisons with previous measurements in argon and x-ray measurements, confirm the choice of this constant to within the experimental error.

IV. RESULTS AND DISCUSSION

a.) Experimental Cross Sections

Single electron capture and loss cross sections were measured as a function of energy for bare nuclei and one-electron ions of carbon, nitrogen, oxygen, and fluorine incident on helium gas. The cross sections were extracted by the "initial growth method" and the results of these measurements and their uncertainties are given in Tables 4-1 to 4-4. The results can also be seen in graphical form in Figures 7 to 10 where the cross sections are plotted as a function of incident ion energy. The solid lines in the figures are drawn to guide the eye.

In general, the single electron capture cross sections fall off by several orders of magnitude over the energy range of interest for the various incident ions used. The single electron loss or ionization cross sections exhibit a very broad maximum over the energy range of this work, that is, near the peak of the cross section. The general shape of the ionization curves can be understood qualitatively by the following. At low incident energies, i.e. small relative velocities, the cross section increases with energy because of the increased momentum transfer available to the electron of interest. At high energies, the cross section decreases with increasing energy because the interaction time between the projectile and target atoms is becoming appreciably smaller. The peak of the cross section occurs when the ion velocity and the velocity of the electron that is to be ionized are approximately equal.

Tables 4-1 to 4-4 Single electron transfer cross sections, σ_{ij}, for carbon, nitrogen, oxygen, and fluorine incident on helium gas. The cross sections are given over a range of energies, with their relative uncertainties, in units of cm^2/atom.

Table 4-1

$C^{+q} \rightarrow He$; cross sections, σ_{ij}, in cm^2/atom
with relative uncertainties

Energy (MeV)	σ_{65}	σ_{54}	σ_{56}
6.03	$2.49 \times 10^{-17} \pm .15$	$1.36 \times 10^{-17} \pm .07$	$5.07 \times 10^{-19} \pm .52$
8.33	$7.78 \times 10^{-18} \pm .65$	$4.01 \times 10^{-18} \pm .28$	$6.60 \times 10^{-19} \pm .67$
10.5	$2.87 \times 10^{-18} \pm .14$	$1.42 \times 10^{-18} \pm .07$	$6.10 \times 10^{-19} \pm .32$
12.0	$1.77 \times 10^{-18} \pm .17$	$8.68 \times 10^{-19} \pm .37$	$7.23 \times 10^{-19} \pm .48$
13.58	$8.13 \times 10^{-19} \pm .46$	$3.61 \times 10^{-19} \pm .22$	$8.23 \times 10^{-19} \pm .44$
16.0	$5.72 \times 10^{-19} \pm .39$	$2.62 \times 10^{-19} \pm .18$	$7.78 \times 10^{-19} \pm .35$
18.5	$2.87 \times 10^{-19} \pm .18$	$1.41 \times 10^{-19} \pm .09$	$6.71 \times 10^{-19} \pm .24$
18.75	$2.81 \times 10^{-19} \pm .27$	$1.34 \times 10^{-19} \pm .09$	$6.83 \times 10^{-19} \pm .35$
20.5	$2.08 \times 10^{-19} \pm .15$	$9.12 \times 10^{-19} \pm .54$	$6.52 \times 10^{-19} \pm .22$
22.5	$1.28 \times 10^{-19} \pm .13$	$6.43 \times 10^{-20} \pm .50$	$6.24 \times 10^{-19} \pm .22$
24.12	$1.08 \times 10^{-19} \pm .09$	$4.61 \times 10^{-20} \pm .46$	$6.49 \times 10^{-19} \pm .33$
25.5	$8.39 \times 10^{-20} \pm .75$	$3.36 \times 10^{-20} \pm .46$	$6.00 \times 10^{-19} \pm .18$

Table 4-2

$N^{+q} \rightarrow He$; cross sections, σ_{ij}, in cm^2/atom
with relative uncertainties

Energy (MeV)	σ_{76}	σ_{65}	σ_{67}
5.17	$8.22 \times 10^{-17} \pm .95$	$5.21 \times 10^{-17} \pm .34$	-------
7.14	$3.74 \times 10^{-17} \pm .21$	$2.20 \times 10^{-17} \pm .08$	$2.16 \times 10^{-19} \pm .40$
11.64	$5.20 \times 10^{-18} \pm .29$	$3.41 \times 10^{-18} \pm .12$	$3.71 \times 10^{-19} \pm .32$
14.0	$2.54 \times 10^{-18} \pm .10$	-------	-------
16.1	$1.44 \times 10^{-18} \pm .07$	$7.67 \times 10^{-19} \pm .33$	$4.03 \times 10^{-19} \pm .29$
20.69	$5.53 \times 10^{-19} \pm .31$	$2.84 \times 10^{-19} \pm .20$	$3.92 \times 10^{-19} \pm .28$
25.1	$2.54 \times 10^{-19} \pm .18$	$1.45 \times 10^{-19} \pm .08$	$4.06 \times 10^{-19} \pm .19$

Table 4-3

$O^{+q} \rightarrow He$; cross sections, σ_{ij}, in cm^2/atom
with relative uncertainties

Energy (MeV)	σ_{87}	σ_{76}	σ_{78}
9	$3.51 \times 10^{-17} \pm .26$	$2.40 \times 10^{-17} \pm .12$	$1.25 \times 10^{-19} \pm .13$
16	$4.33 \times 10^{-18} \pm .14$	$2.48 \times 10^{-18} \pm .07$	$1.90 \times 10^{-19} \pm .19$
20	$1.63 \times 10^{-18} \pm .10$	$9.43 \times 10^{-19} \pm .03$	$2.36 \times 10^{-19} \pm .21$
25	$6.37 \times 10^{-19} \pm .17$	$3.82 \times 10^{-19} \pm .24$	$2.48 \times 10^{-19} \pm .17$
30	$2.89 \times 10^{-19} \pm .15$	$1.59 \times 10^{-19} \pm .07$	$2.07 \times 10^{-19} \pm .18$
36	$1.28 \times 10^{-19} \pm .10$	$7.57 \times 10^{-20} \pm .46$	$2.62 \times 10^{-19} \pm .11$
40	$8.56 \times 10^{-20} \pm 1.02$	$5.01 \times 10^{-20} \pm .27$	$2.49 \times 10^{-19} \pm .08$

Table 4-4

$F^{+q} \rightarrow He$; cross sections, σ_{ij}, in cm^2/atom
with relative uncertainties

Energy (MeV)	σ_{98}	σ_{87}	σ_{89}
10.7	$4.40 \times 10^{-17} \pm .19$	$3.48 \times 10^{-17} \pm .11$	$6.14 \times 10^{-20} \pm 1.13$
13	$2.24 \times 10^{-17} \pm .09$	$1.74 \times 10^{-17} \pm .06$	$5.90 \times 10^{-20} \pm 1.08$
16	$9.39 \times 10^{-18} \pm .34$	$7.73 \times 10^{-18} \pm .36$	$1.23 \times 10^{-19} \pm .19$
19	$5.26 \times 10^{-18} \pm .23$	$3.72 \times 10^{-18} \pm .14$	$1.07 \times 10^{-19} \pm .13$
22	$2.75 \times 10^{-18} \pm .13$	$1.98 \times 10^{-18} \pm .22$	$1.13 \times 10^{-19} \pm .26$
25	$1.75 \times 10^{-18} \pm .06$	$1.22 \times 10^{-18} \pm .03$	$1.08 \times 10^{-19} \pm .10$
27	$1.20 \times 10^{-18} \pm .05$	$8.23 \times 10^{-19} \pm .25$	$1.55 \times 10^{-19} \pm .16$
29.7	$8.99 \times 10^{-19} \pm .56$	$5.84 \times 10^{-19} \pm .31$	$1.58 \times 10^{-19} \pm .10$
32	$5.61 \times 10^{-19} \pm .31$	$4.04 \times 10^{-19} \pm .09$	$1.45 \times 10^{-19} \pm .06$
35	$3.50 \times 10^{-19} \pm .31$	-------	$1.53 \times 10^{-19} \pm .37$
41	$2.24 \times 10^{-19} \pm .19$	$1.32 \times 10^{-19} \pm .08$	$1.55 \times 10^{-19} \pm .21$
47	$1.40 \times 10^{-19} \pm .06$	$8.28 \times 10^{-20} \pm .59$	$1.70 \times 10^{-19} \pm .02$

Figures 7-10 The single charge transfer cross sections for the bare nuclei and one-electron ions of carbon, nitrogen, oxygen, and fluorine incident on helium gas. The cross sections are given in units of cm^2/atom, as a function of projectile energy. The solid curves are drawn to guide the eye.

Figure 7

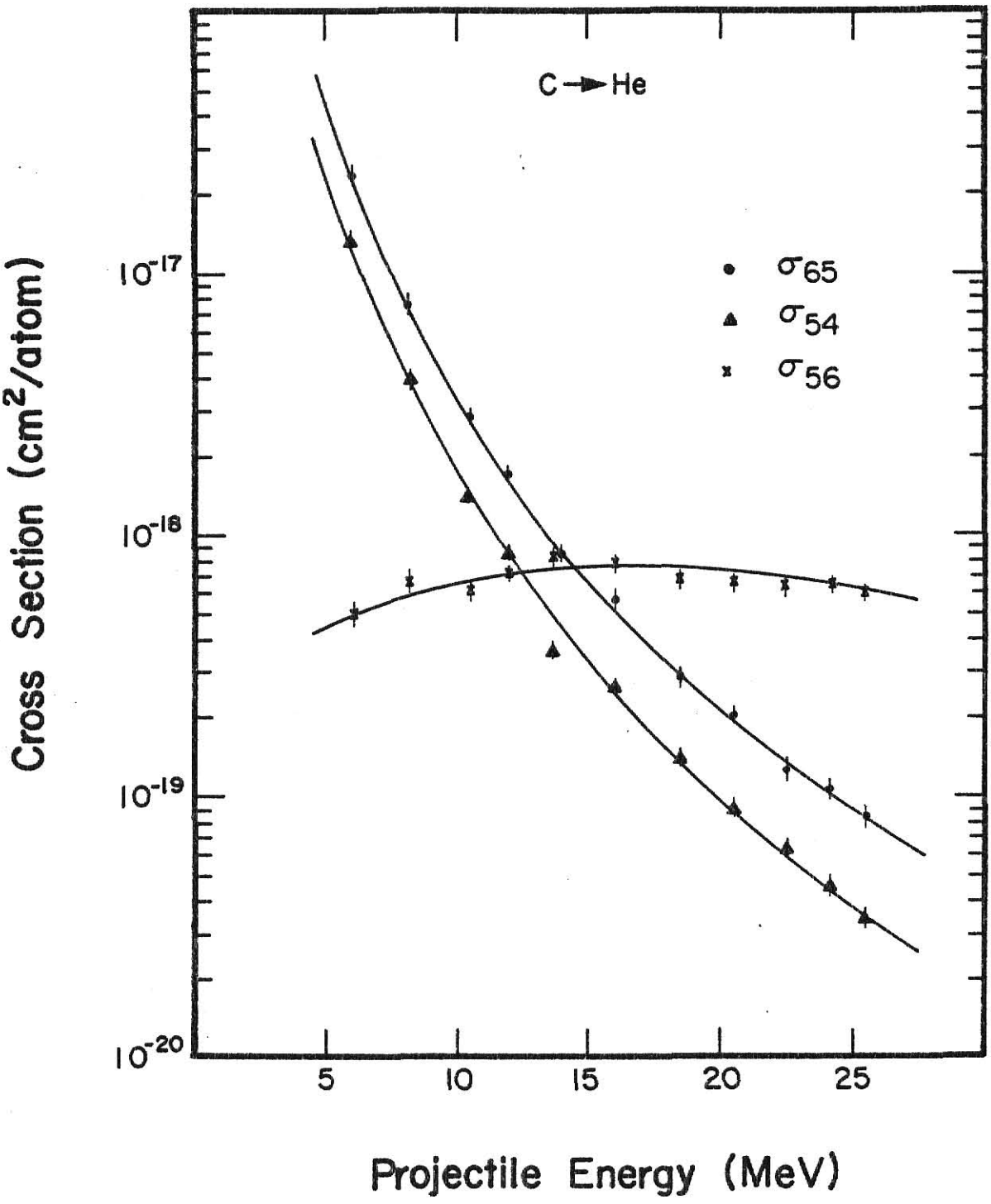
C → He
σ65
σ54
σ56
Cross Section (cm²/atom)
10⁻¹⁷
10⁻¹⁸
10⁻¹⁹
10⁻²⁰
5
10
15
20
25
Projectile Energy (MeV)

Figure 8

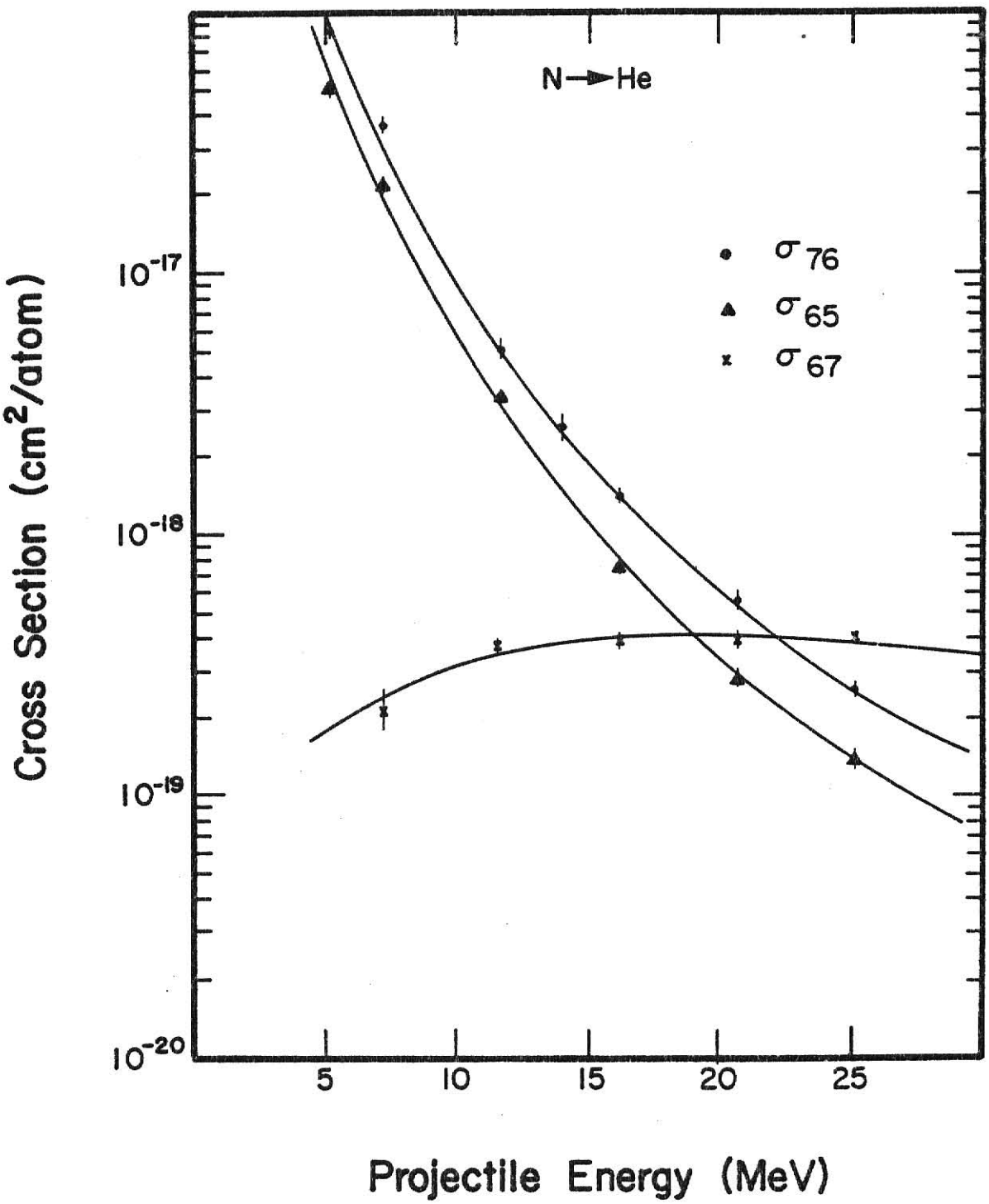
N→He
σ76
σ65
σ67
10-17
10-18
10-19
10-20
5
10
15
20
25
Cross Section (cm2/atom)
Projectile Energy (MeV)

Figure 9

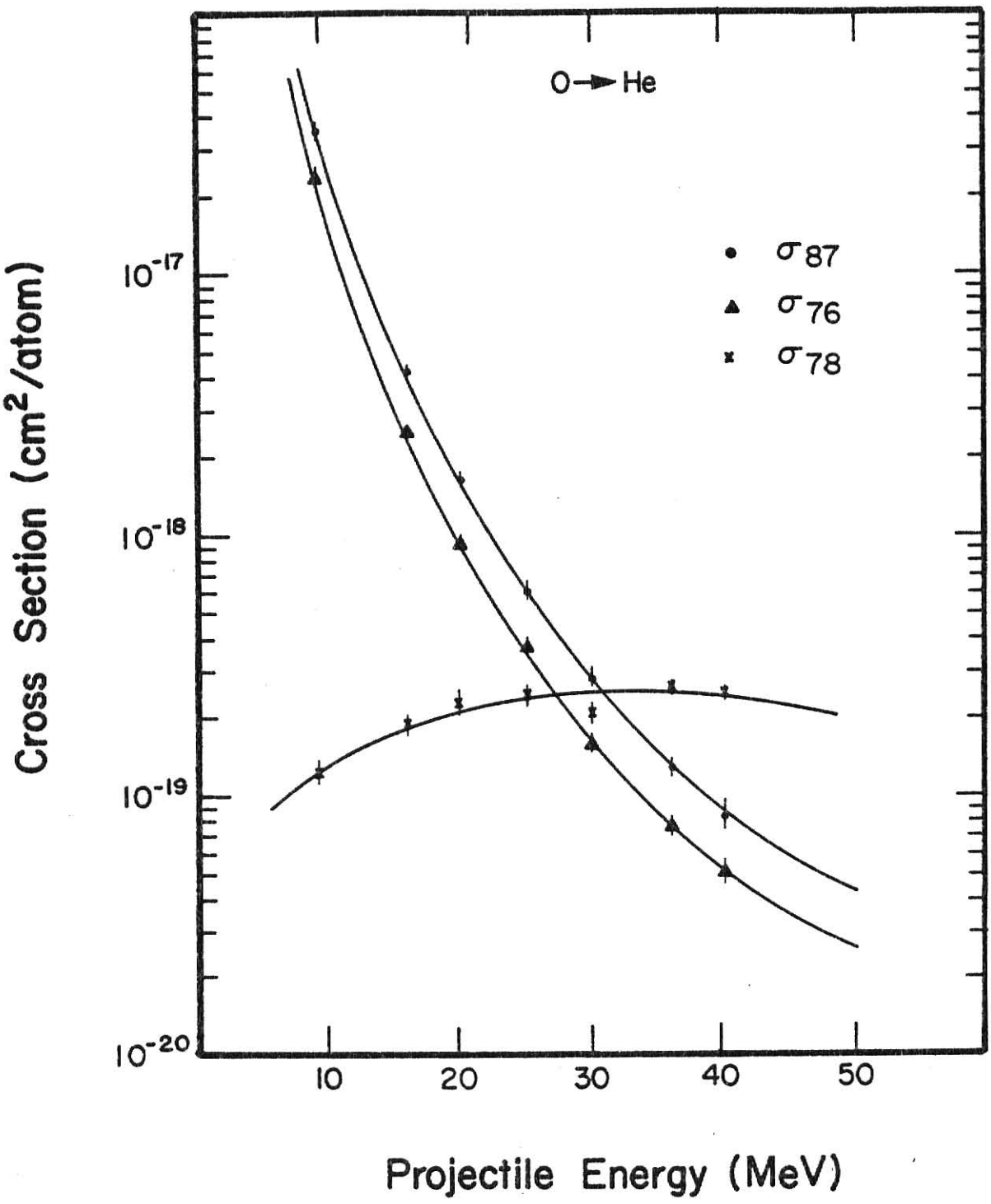
O→He
σ_{87}
σ_{76}
σ_{78}
Cross Section (cm^2/atom)
10^{-17}
10^{-18}
10^{-19}
10^{-20}
10
20
30
40
50
Projectile Energy (MeV)

Figure 10

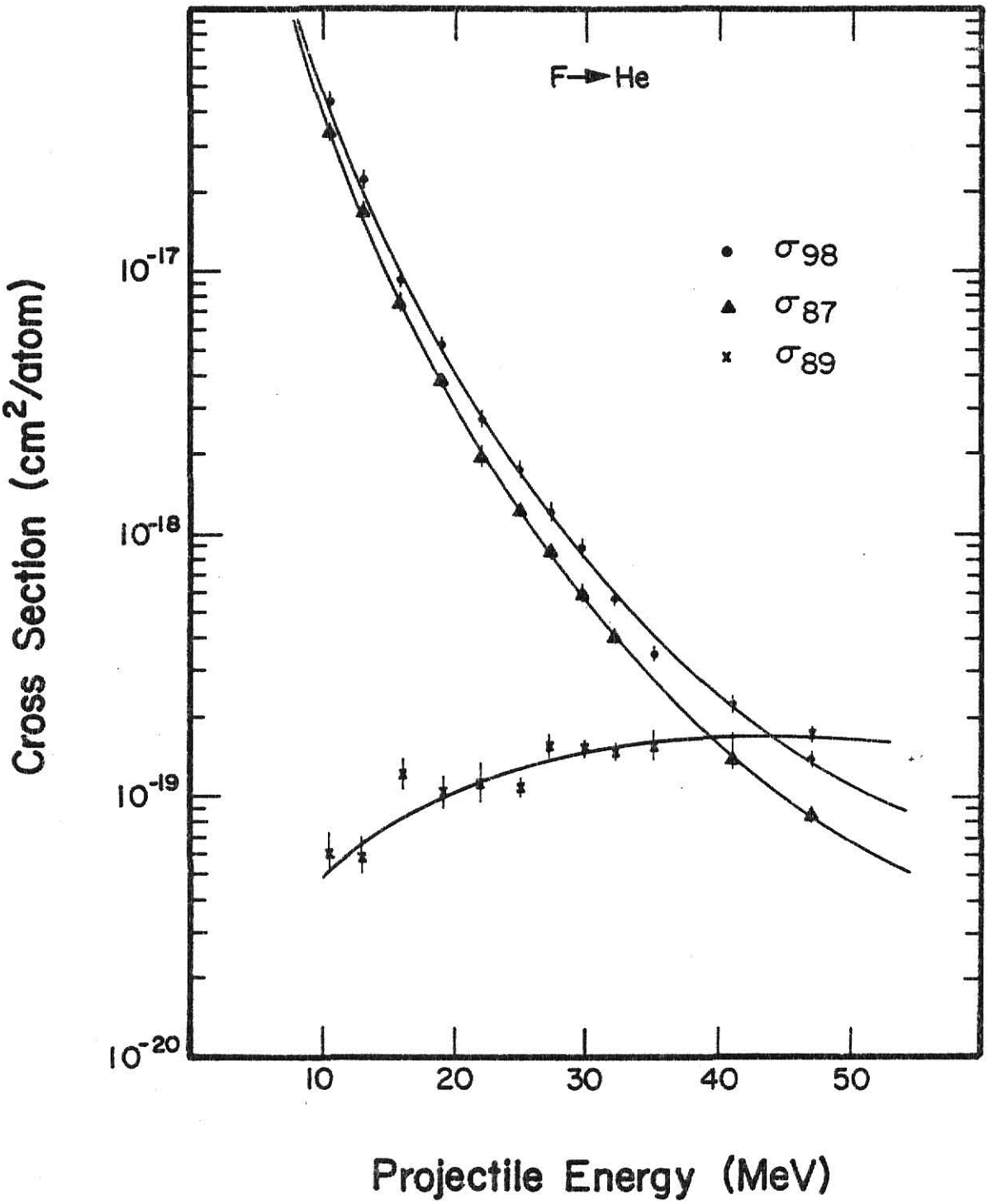
F→He
σ_{98}
σ_{87}
σ_{89}
Cross Section (cm²/atom)
10⁻¹⁷
10⁻¹⁸
10⁻¹⁹
10⁻²⁰
10
20
30
40
50
Projectile Energy (MeV)

b.) Comparison with PWBA for Electron Loss

Ionization cross sections have been computed utilizing the PWBA calculation for the one-electron ions of C, N, O, and F incident on He gas. The calculation utilizes the results of protons on hydrogen scaled by the factor Z_1^2/Z_2^4, where Z_1 and Z_2 are the atomic numbers of the projectile and target atoms respectively. The results of this calculation are compared to the experimentally determined cross sections for ionization in Figure 11, where the curves represent the PWBA calculation for the various ions. As can be seen from the figure, the agreement between the experimental results and the PWBA calculation are excellent, within the limits of the experimental error. The close agreement between the two indicates that the PWBA calculation accurately describes the simple systems chosen for this experiment without the use of correction terms used by other workers.[20] Also, the comparison shows that the cross sections do indeed scale by the factor Z_1^2/Z_2^4, and the absolute magnitude of the curves for the various values of Z_2 are correct.

In Figure 12, the PWBA curves for the ions of interest are compared to the PWBA with Coulomb deflection and binding energy corrections.[20] In general, the corrections due to Coulomb deflection are much less than 1%, while the binding energy correction is significant. At low energies, the binding energy correction lowers the cross section by about 40%, while at high energies, the cross section is lowered by approximately 10%. In addition to the Coulomb deflection and binding energy corrections, one can also include a polarization correction term.[20] The comparison between the PWBA with the three corrections (PWBABCP), and the experimental results is shown in Figure 13. Once again, the agreement is good, within

Figure 11 The ionization cross sections for the one-electron ions of carbon, nitrogen, oxygen and fluorine incident on helium gas. The cross sections are in units of cm^2/atom, and are given as a function of projectile energy. The solid curves represent a theoretical PWBA calculation.

Figure 11

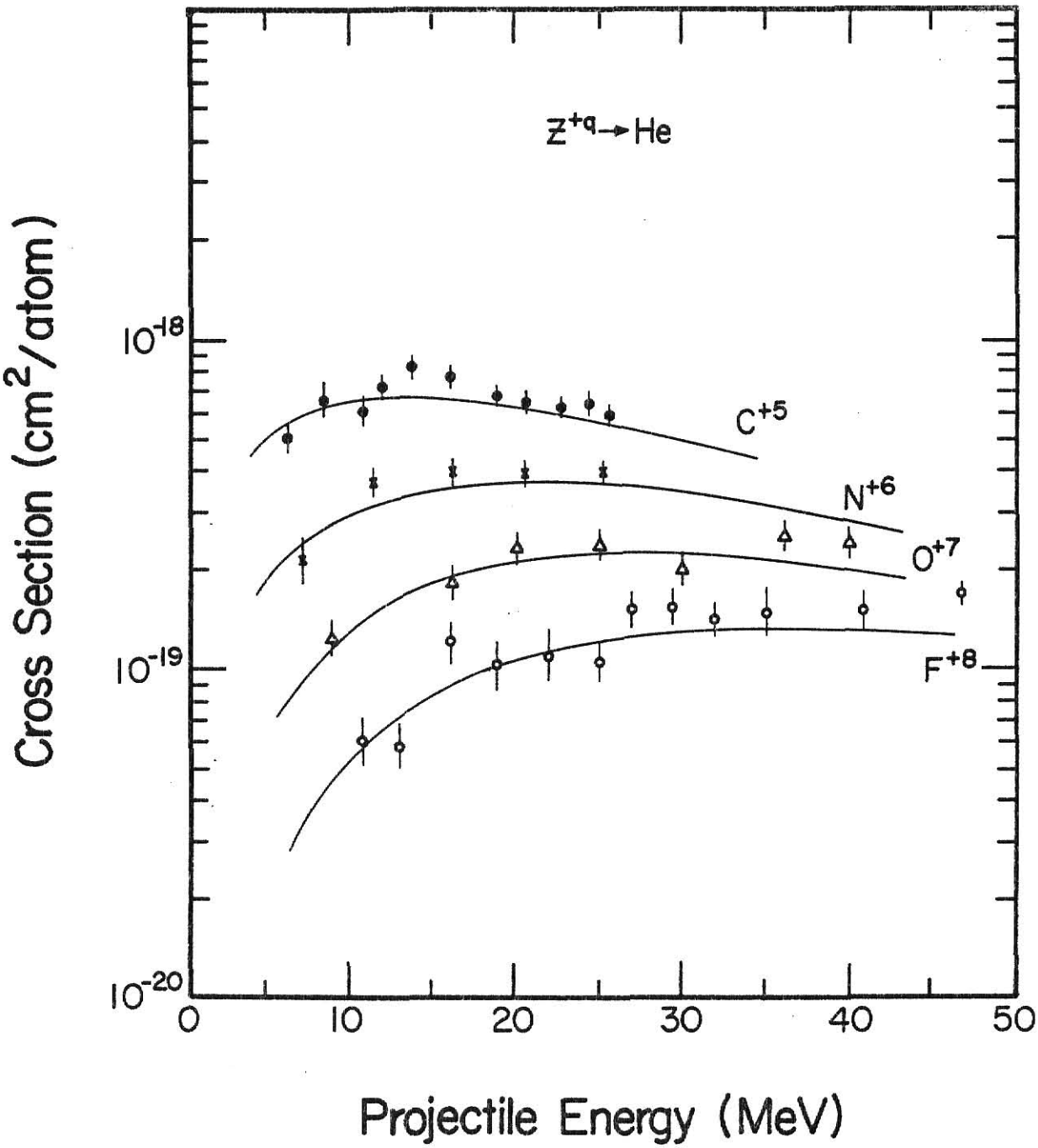
$Z^{+q} \rightarrow He$
C^{+5}
N^{+6}
O^{+7}
F^{+8}
Cross Section (cm^2/atom)
10^{-18}
10^{-19}
10^{-20}
0
10
20
30
40
50
Projectile Energy (MeV)

Figure 12 The theoretical PWBA curves for the ions of interest (solid curves in the figure) are compared to the PWBA with Coulomb deflection and binding energy corrections (dashed curves in the figure).

Figure 12

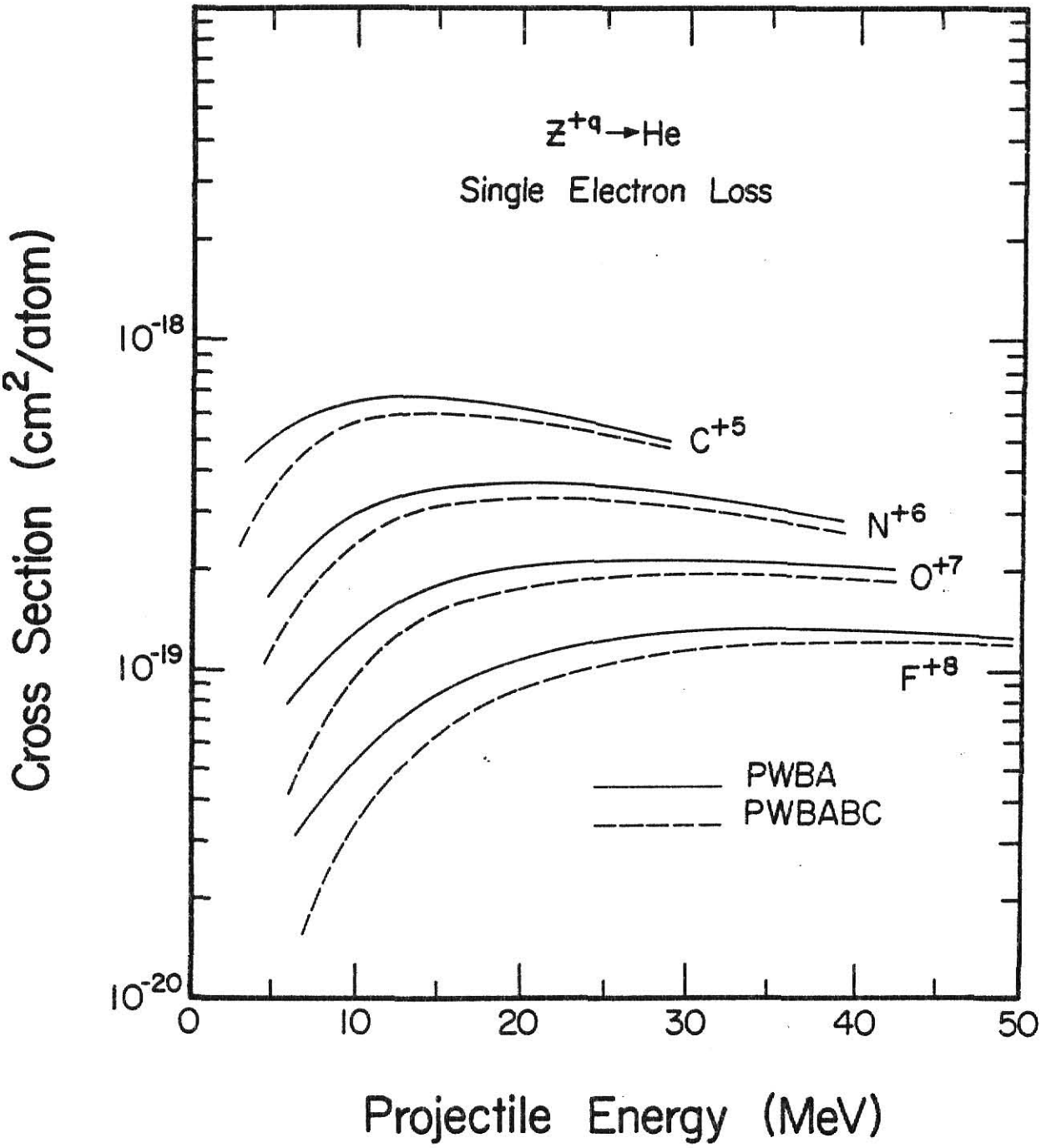
$Z^{+q} \rightarrow He$
Single Electron Loss
Cross Section (cm^2/atom)
10^{-18}
10^{-19}
10^{-20}
C^{+5}
N^{+6}
O^{+7}
F^{+8}
PWBA
PWBABC
0
10
20
30
40
50
Projectile Energy (MeV)

Figure 13 A comparison between the ionization cross sections and the theoretical PWBA with Coulomb deflection, binding energy, and polarization corrections (PWBABCP).

Figure 13

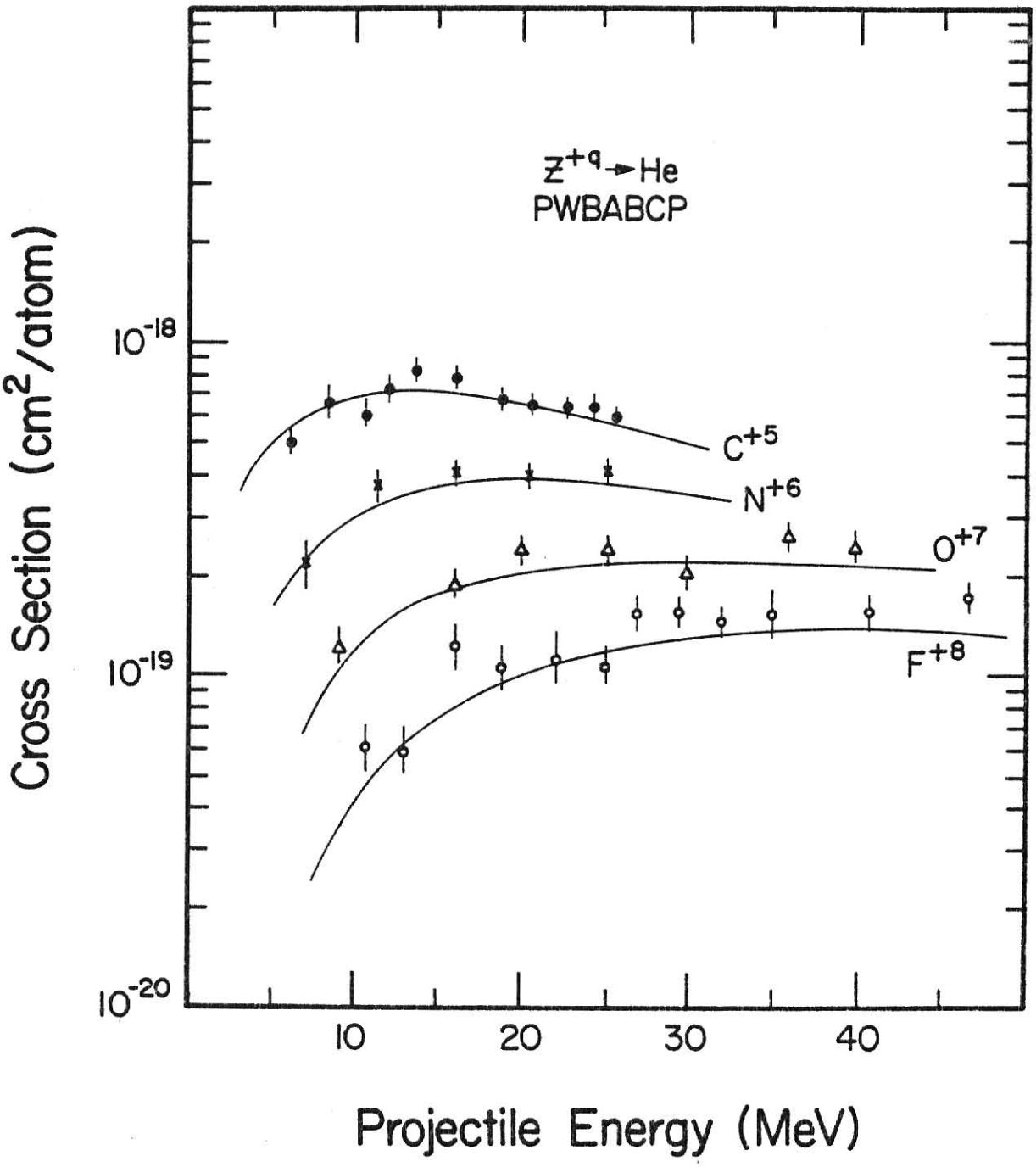
$Z^{+q} \rightarrow He$
PWBABCP
C^{+5}
N^{+6}
O^{+7}
F^{+8}
10^{-18}
10^{-19}
10^{-20}
Cross Section (cm^2/atom)
10
20
30
40
Projectile Energy (MeV)

the experimental error. However, the present work shows that these corrections are not necessary in order to obtain agreement between theory and experiment. The PWBA calculation, in which no correction terms are included, gives good agreement with experimental results.

c.) Comparison with X-ray Cross Sections for Electron Capture

Following electron capture, x-ray production may result by a de-excitation process, if the capture was to an excited state of the atom. Figure 14 shows a typical example of the x-ray cross sections of Guffey,[22] represented by a dashed line, as compared to the single electron capture cross sections of this work, the solid line in the figure. The data is for bare oxygen incident on helium gas and is given as a function of projectile energy. In general, at low energies the x-ray cross sections are approximately 70% of the capture cross sections. However, one sees that the x-ray cross sections fall more rapidly with energy than do the capture cross sections.

The x-ray and capture cross sections were also compared through the use of the function $g(Z_1,E)$ from Eq. (2-23). Figures 15 through 18 show $g(Z_1,E)$ from a Brinkman-Kramers calculation (dashed curves in the figures), compared to the same function using the capture cross sections of this work (solid curves in the figures). It is clear from the figures that the ratio of x-ray to capture cross sections obtained through a Brinkman-Kramers calculation do not agree with experimental results. This comparison shows that the single normalization constant for capture to each state, which was used in the theoretical analysis of the x-ray cross sections, is inadequate. In particular, the present results show that

Figure 14 A comparison between the single electron capture and x-ray cross sections for $O^{+8} \rightarrow He$. The cross sections are in units of cm^2/atom and are given as a function of projectile energy.

Figure 14

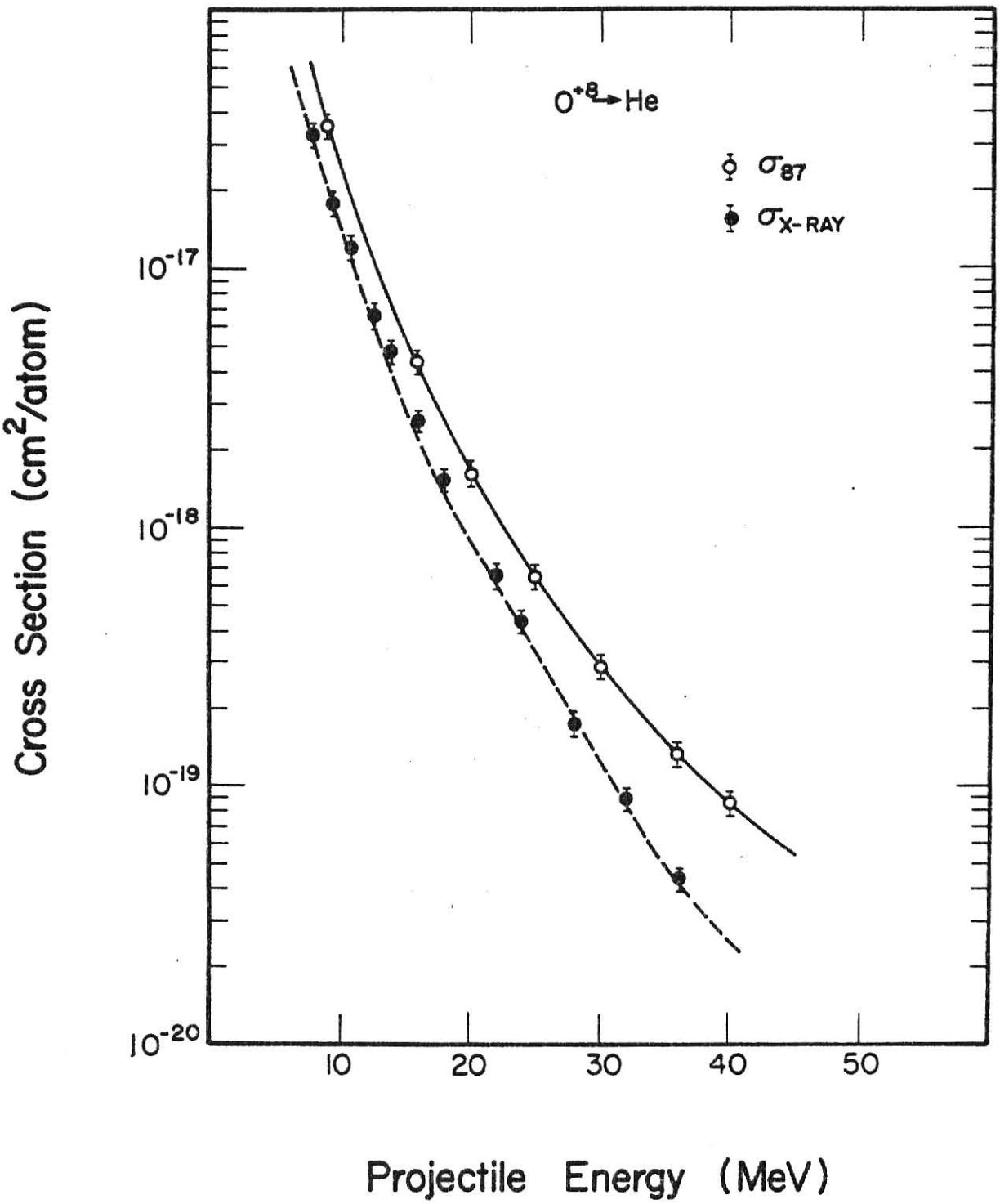
$O^{+8} \rightarrow He$
σ_{87}
$\sigma_{X\text{-}RAY}$
Cross Section (cm^2/atom)
10^{-17}
10^{-18}
10^{-19}
10^{-20}
10
20
30
40
50
Projectile Energy (MeV)

Figures 15-18 The function $g(Z_1,E)$ calculated from a Brinkman-Kramers forumlation (dashed lines in the figures) as compared to the same function found utilizing the capture cross sections of this work (solid lines in the figures).

Figure 15

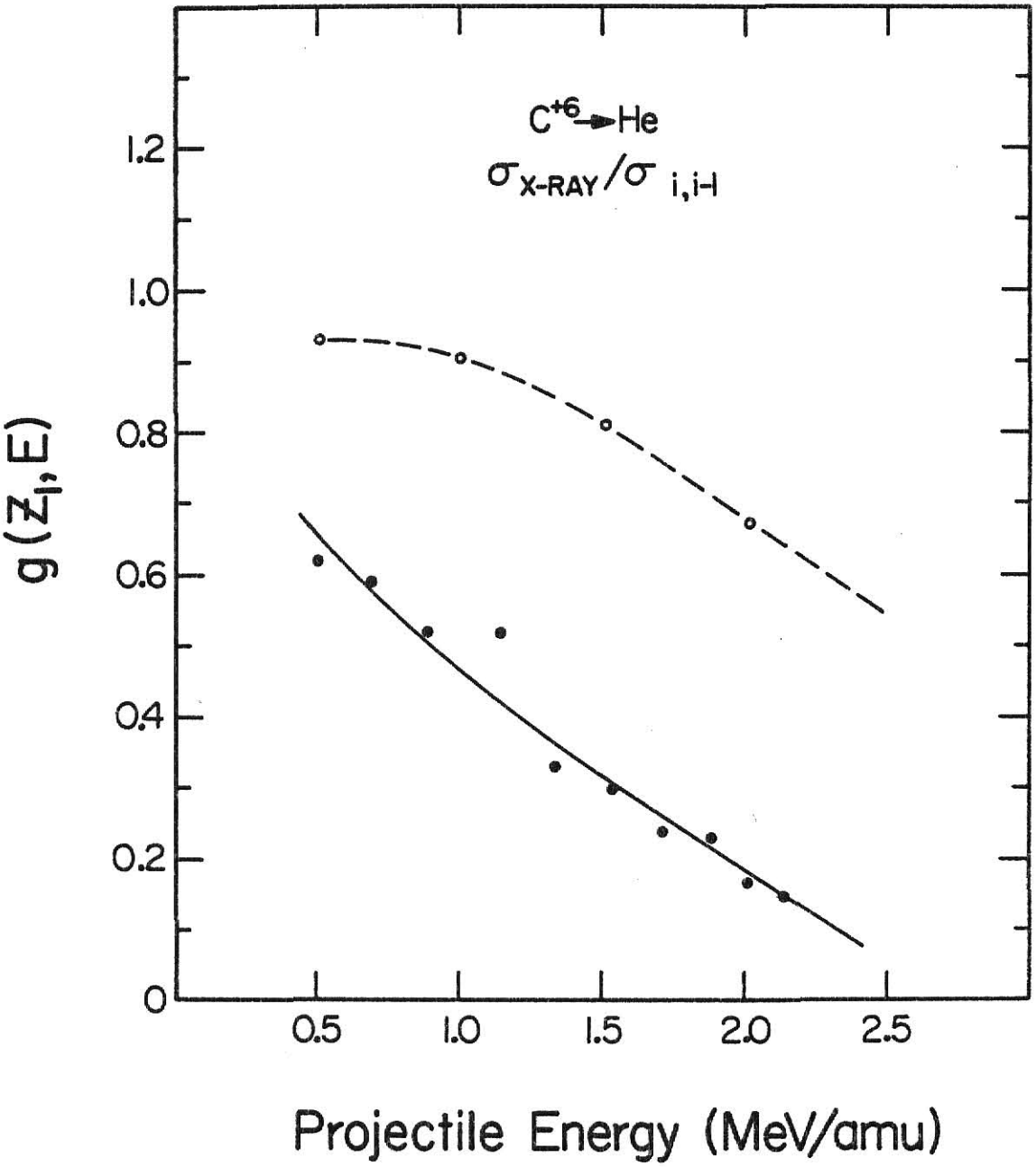
C+6→He
σX-RAY/σ i,i-H
g(Zi,E)
1.2
1.0
0.8
0.6
0.4
0.2
0
0.5
1.0
1.5
2.0
2.5
Projectile Energy (MeV/amu)

Figure 16

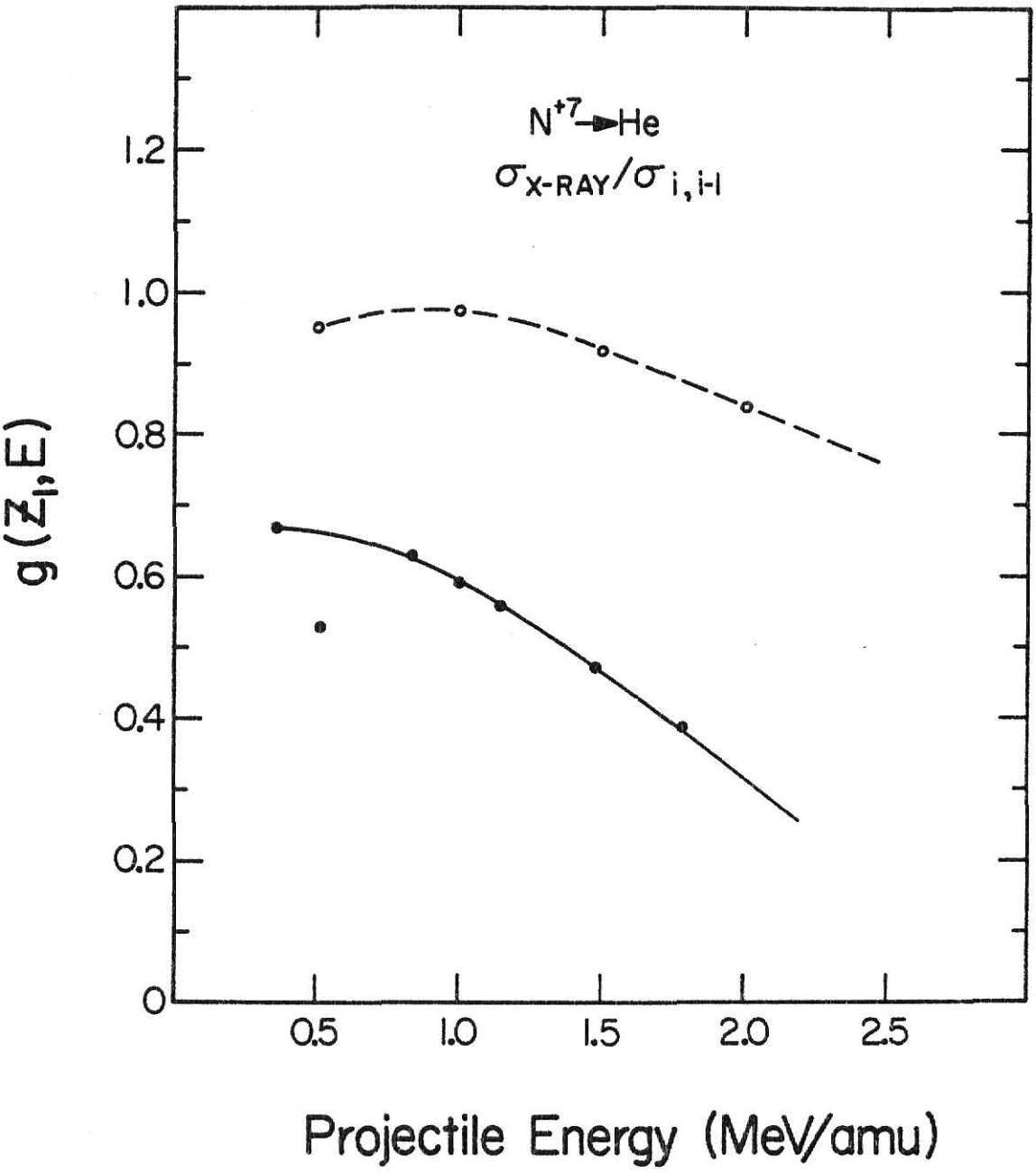
$N^{+7} \rightarrow He$
$\sigma_{X\text{-}RAY}/\sigma_{i,i-1}$
g(Z1,E)
1.2
1.0
0.8
0.6
0.4
0.2
0
0.5
1.0
1.5
2.0
2.5
Projectile Energy (MeV/amu)

Figure 17

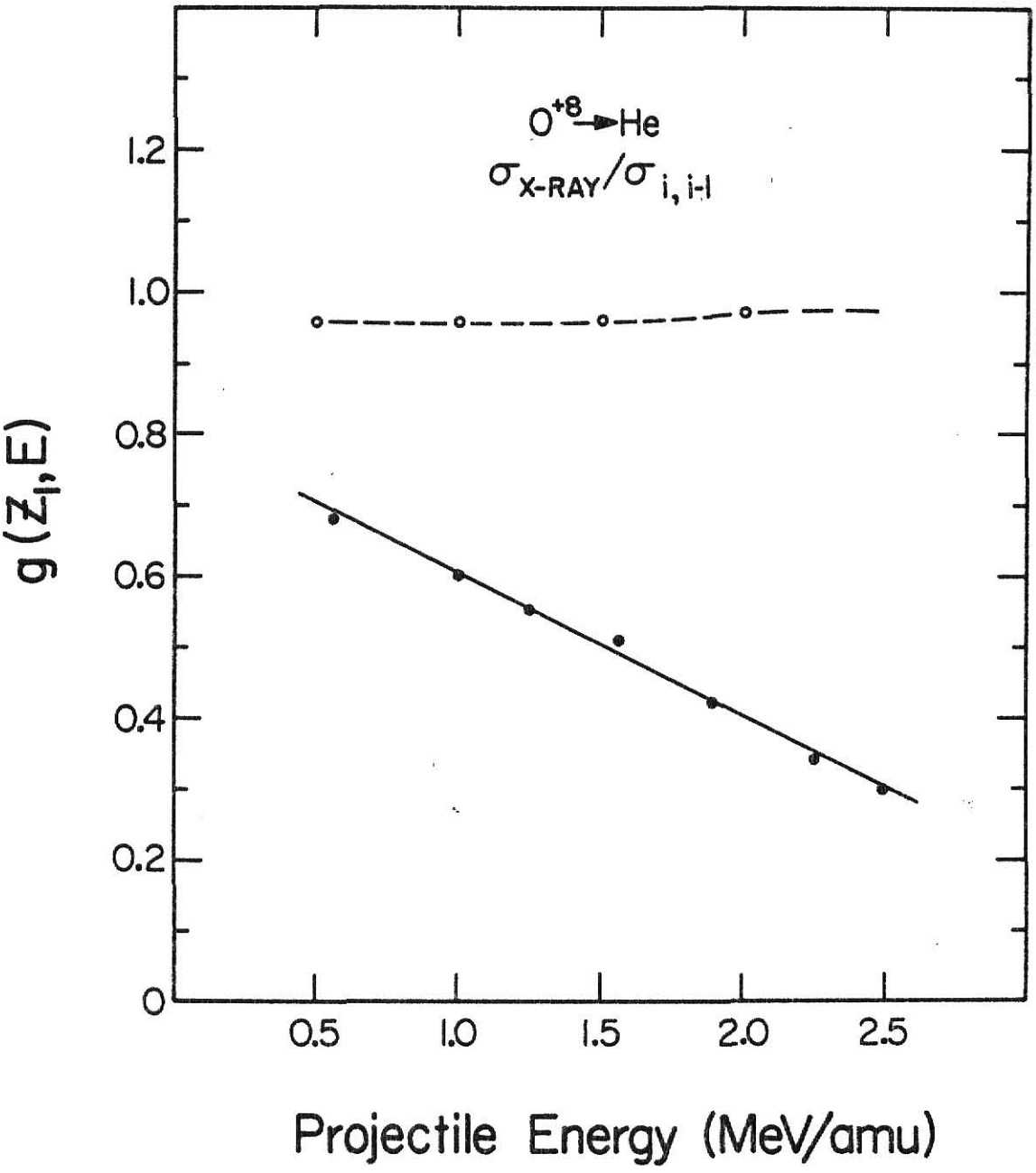
$O^{+8} \rightarrow He$
$\sigma_{X\text{-}RAY}/\sigma_{i,i-1}$
g (Z1, E)
1.2
1.0
0.8
0.6
0.4
0.2
0
0.5
1.0
1.5
2.0
2.5
Projectile Energy (MeV/amu)

Figure 18

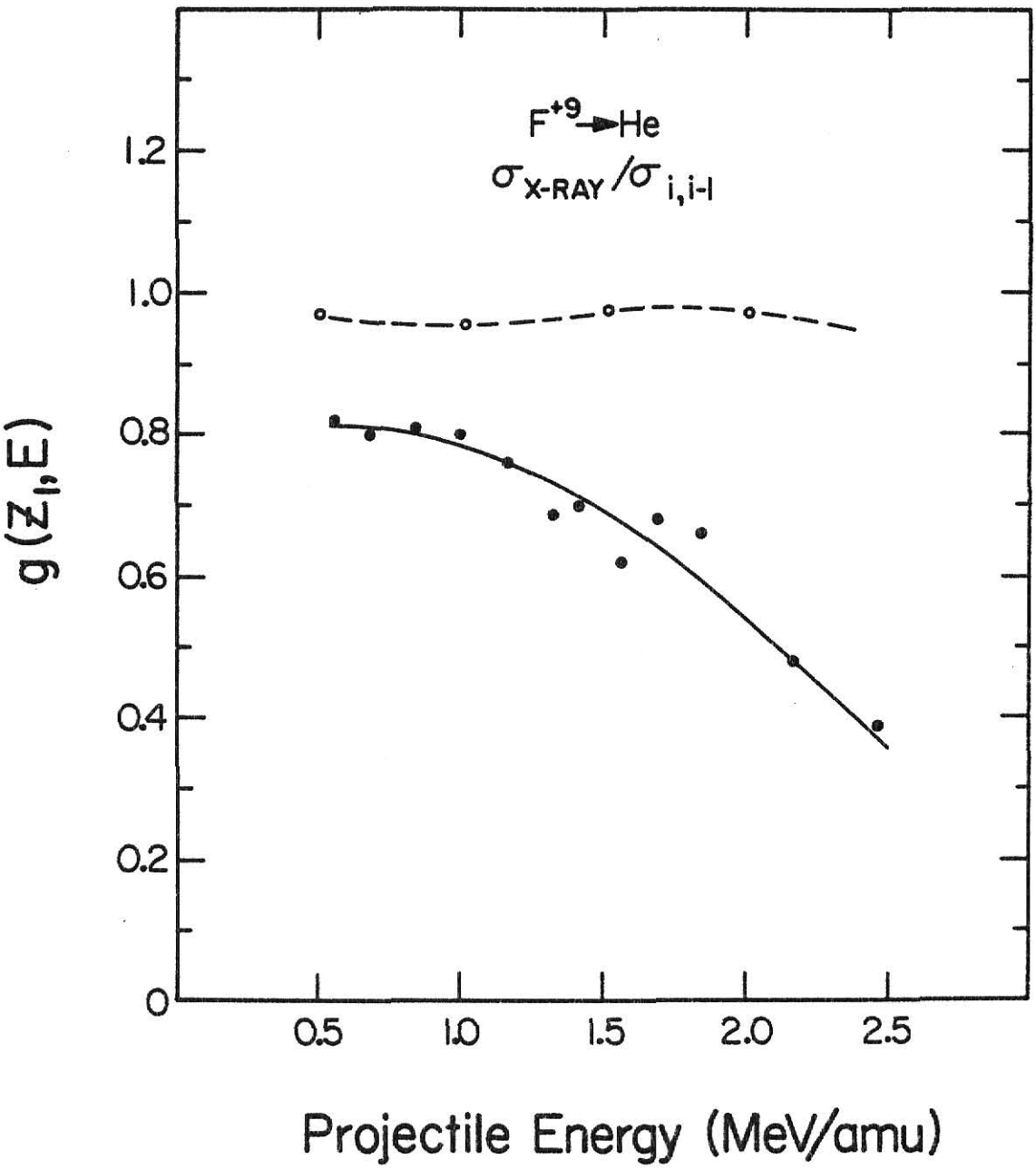
F+9 → He
σX-RAY / σ i,i-1
g (Z1, E)
1.2
1.0
0.8
0.6
0.4
0.2
0
0.5
1.0
1.5
2.0
2.5
Projectile Energy (MeV/amu)

the B-K calculation underestimates the capture of the electron to the 1s and 2s states as compared to the higher, x-ray emitting states.

Comparisons can also be made between the x-ray and capture cross sections for the one-electron projectiles incident on helium gas. This comparison is shown in Figure 19. In this figure, there is an added feature in that the two curves cross over. This feature can be understood qualitatively in terms of the electron already present on the projectile. Not only can the capture of an electron by the projectile give rise to K x-rays, but also the excitation of the electron already present on the projectile can contribute to the total x-ray cross section. The latter contribution increases rapidly with increasing energy towards a maximum which occurs when the velocity of the projectile and the mean velocity of the K-shell electron are approximately equal. Hence, the single electron capture and total x-ray curves cross over for the one-electron projectiles.

Figure 19 A comparison between the single electron capture and x-ray cross sections for $O^{+7} \rightarrow He$. The cross sections are in units of cm^2/atom and are given as a function of projectile energy.

Figure 19

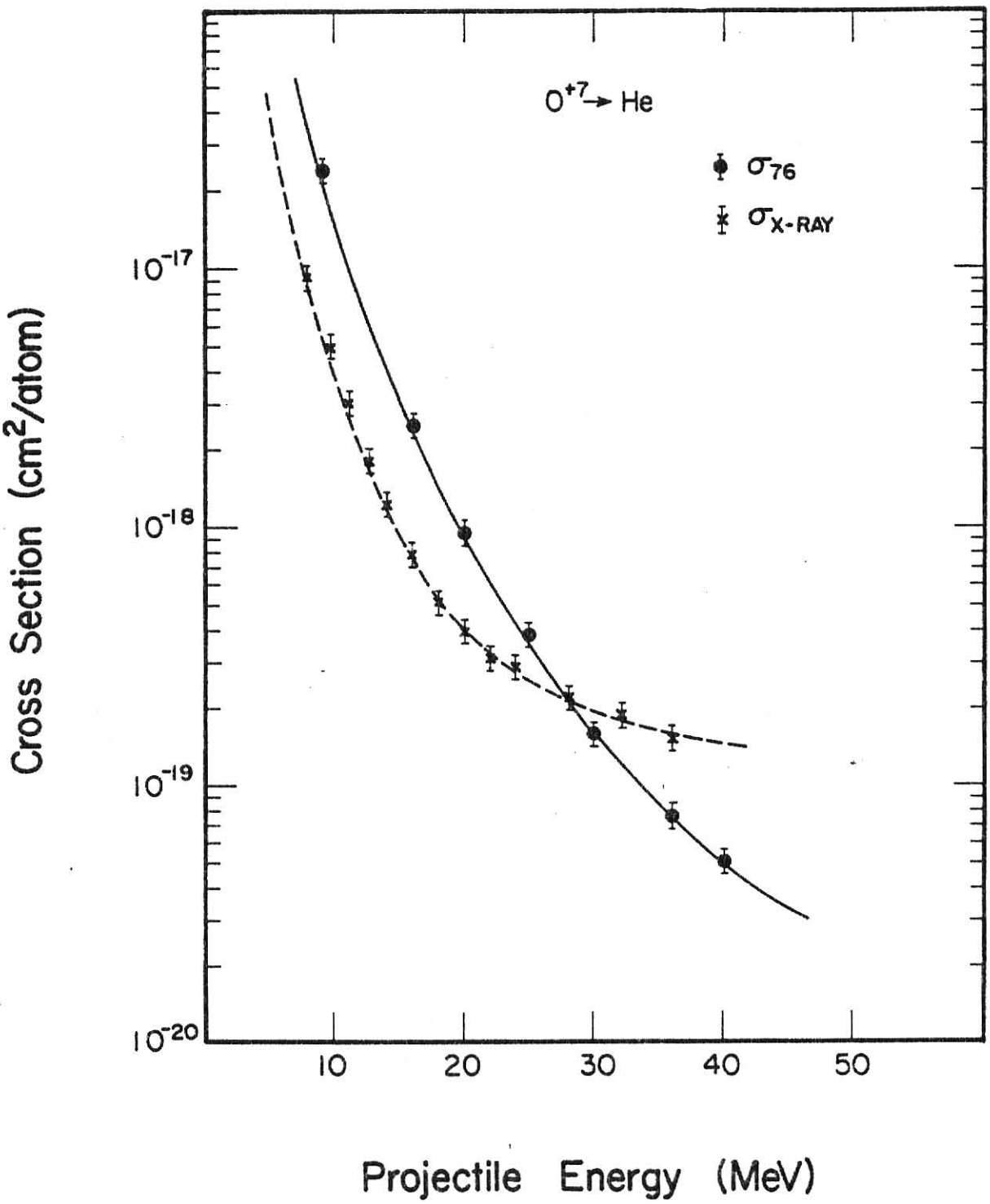
$O^{+7} \rightarrow He$
σ_{76}
$\sigma_{X\text{-}RAY}$
10^{-17}
10^{-18}
10^{-19}
10^{-20}
10
20
30
40
50
Cross Section (cm^2/atom)
Projectile Energy (MeV)

V. SUMMARY

Single electron capture and loss cross sections have been experimentally measured for bare nuclei and one-electron ions of carbon, nitrogen, oxygen, and fluorine incident on helium gas. The cross sections were measured as a function of energy in the range of $\sim$0.5 - 2.5 MeV/amu. Low target gas pressures were utilized to extract charge transfer cross sections by the "initial growth method." In general, single capture cross sections fall off by several orders of magnitude with increasing projectile energy. The ionization cross sections, however, exhibit a very broad maximum over the range of interest.

Comparisons have been made between the ionization cross sections for the various ions and a theoretical PWBA calculation. The PWBA calculation utilizes the results of protons on hydrogen scaled by the factor Z_1^2/Z_2^4. For the hydrogen-like ions used, the agreement between the experimental results and the theoretical calculation is remarkably good. The PWBA cross sections are lowered by approximately 40% at low energies, and 10% at high energies by including Coulomb deflection and binding energy corrections in the calculation. Hence, the PWBABC does not give good agreement with the experimental results. With the additional correction from polarization, the agreement is once again good. However, the present results show that these corrections are not necessary in order to obtain agreement between experiment and theory since the PWBA calculation, without the inclusion of any correction terms, gives good agreement. This is contrary to the conclusions in the work of others[20] who have studied ionization of screened K-shell electrons. It should be noted, however, that the ionization process

studied in this work is near the peak of the cross section where the PWBA and PWBABCP results are similar. Figure 20 shows the PWBA calculations with and without the various correction terms over an extended energy range for fluorine on helium. It can be seen from the figure that the curves tend to diverge in the low energy region. Thus measurements of the cross sections at lower energies for one-electron ions would provide a good test for the corrections to the PWBA, but this remains a subject for further investigation.

Single electron capture cross sections were compared to total x-ray cross sections. The results of this comparison confirms the magnitude of the x-ray cross sections to an accuracy of $\sim$30%. A comparison was also made for the ratio of the x-ray cross section to the total capture cross section from this work, to the same ratio calculated from a Brinkman-Kramers formulation. There is not good agreement between experiment and the B-K calculation, showing that the single normalization constant used in the analysis of the x-ray cross sections for capture to each state is inadequate. In particular, the capture of the electron to the 1s and 2s states is underestimated, as compared to the higher x-ray emitting states, in the B-K calculation.

Figure 20 The theoretical PWBA curves with Coulomb deflection, binding energy, and polarization corrections are shown for $F^{+8} \rightarrow He$. The cross sections are given over an extended energy range with the present range indicated by arrows in the figure.

Figure 20

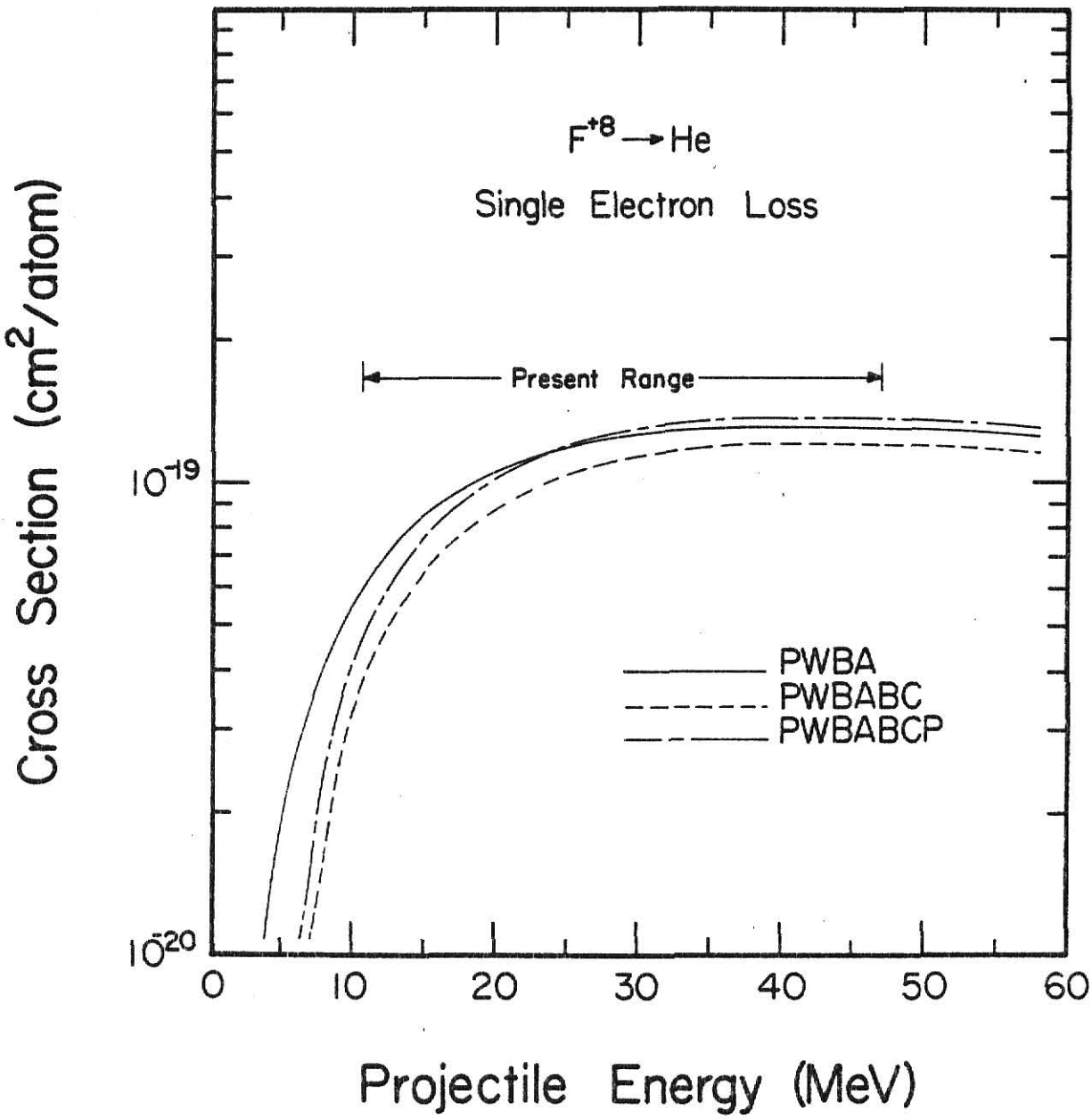
F+8 → He
Single Electron Loss
Present Range
PWBA
PWBABC
PWBABCP
Cross Section (cm²/atom)
10⁻¹⁹
10⁻²⁰
0
10
20
30
40
50
60
Projectile Energy (MeV)

REFERENCES

1. P. Richard, in Atomic Inner-Shell Processes, edited by B. Craseman (Academic Press, New York, 1975), vol. 1, pp. 74-152.

2. C. F. Barnett, invited lecture IX ICPEAC, 1975, The Physics of Electronic and Atomic Collisions, edited by J. S. Risley and R. Geballe, pp. 846-853.

3. G. Steigman, Ap. J. 199, 642 (1975).

4. M. R. C. McDowell and J. P. Coleman, Introduction to the Theory of Ion-Atom Collisions, (North-Holland, Amsterdam, 1970), Chap. 7.

5. J. R. Macdonald and F. W. Martin, Phys. Rev. A 4, 1965 (1971).

6. T. Chiao, Ph.D. Thesis (Kansas State University, 1973).

7. S. K. Allison and M. Garcia-Munoz, in Atomic and Molecular Processes, edited by D. R. Bates (Academic Press, New York, 1962), pp. 721-782.

8. V. S. Nikolaev, Usp. Fiz. Nauk. 85, 679 (1965); Sov. Phys. Usp. 8, 269 (1965).

9. H. D. Betz, Rev. Mod. Phys. 44, 465 (1972).

10. H. Tawara and A. Russek, Rev. Mod. Phys. 45, 178 (1973).

11. J. D. Garcia, R. J. Fortner, and T. M. Kavanagh, Rev. Mod. Phys. 45, 111 (1973).

12. E. Merzbacher and H. W. Lewis, in Encyclopedia of Physics, S. Flugge (Springer-Verlag, Berlin, 1958), Vol. 34, p. 166.

13. J. H. McGuire, private communication.

14. G. Basbas, in Electronic and Atomic Collisions, edited by J. S. Risley and R. Geballe (University of Washington, Seattle, 1975), p. 502.

15. E. Merzbacher, Quantum Mechanics, (John Wiley and Sons, Inc. New York, 1970), Chap. 11.

16. D. R. Bates, in Atomic and Molecular Processes, edited by D. R. Bates (Academic Press, New York, 1962), pp. 549-621.

17. E. Merzbacher and H. W. Lewis, in Encyclopedia of Physics, S. Flugge (Springer-Verlag, Berlin, 1958), Vol. 34, p. 166.

18. J. Golden, Ph.D. thesis (Kansas State University, 1975).

19. J. H. McGuire and M. Patton, private communication.

20. G. Basbas, W. Brandt, and R. Laubert, Phys. Rev. A 7, 983 (1973); G. Basbas, W. Brandt, and R. Laubert, Phys. Rev. A 17, 1655 (1978).

21. G. S. Khandelwal, B. H. Choi, and E. Merzbacher, At. Data 1, 103 (1969).

22. J. A. Guffey, Ph.D. thesis (Kansas State University, 1976); J. A. Guffey, L. D. Ellsworth, and J. R. Macdonald, Phys. Rev. A 15, 1863 (1977).

23. A. M. Halpern, and J. Law, Phys. Rev. A 12, 1776 (1975); K. Omidvar, J. E. Golden, and J. H. McGuire, Phys. Rev. A 13, 500 (1976); C. D. Lin, S. C. Soong, and L. N. Tunnell, Phys. Rev. A 17, 1646 (1978); Dz. Belkic, R. Gayet, and A. Salin, Physics Reports 56, 281 (1979).

24. S. K. Allison, Revs. Modern Phys. 30, 1137 (1958).

25. J. Shapiro and G. Breit, Phys. Rev. 113, 179 (1959); U. S. Department of Commerce, National Bureau of Standards, Atomic Transition Probabilities, NSRDS-NBS 4 Vol. 1, pp. 1-6, 1966; C. D. Lin, W. R. Johnson, and A. Dalgarno, Phys. Rev. A 15, 154 (1977); G. W. F. Drake, Phys. Rev. A 3, 908 (1971); T. W. Tunnell, C. P. Bhalla, and C. Can, Phys. Lett. A, to be published; I. A. Sellin, B. L. Donnally, and C. Y. Fan, Phys. Rev. Lett. 21, 717 (1968); A. Dalgarno, The Menzel Symposium, NBS Spec. Publ. No. 353 (U.S. GPO, Washington, D.C., 1971), p. 47.

26. Granville-Phillips Company, Boulder, Colorado.

27. P. R. Bevington, Data Reducation and Error Analysis for the Physical Sciences, (McGraw-Hill, New York, 1969), Chap. 6.

28. L. Weaver, private communication.

APPENDIX 1

The following table lists the PWBA ionization cross section as a function of velocity (or eV/amu) for p + H(1s) → p + p + e. Cross sections for bare ions on other hydrogen systems may be computed using the scaling law, namely

$$\sigma(Z_1, Z_2, v_{inc}) = \frac{Z_1^2}{Z_2^4}\,\sigma(1, 1, v_{inc}/Z_2)$$

where Z_1 is the projectile charge, Z_2 the target charge, and v_{inc} is the relative velocity. $\sigma(1, 1, v)$ is tabulated here.

Example: 25.6 MeV $O^{+7}(1s) + He^{+2} \rightarrow O^{+8} + He^{+2} + e$. Calculation of v_{inc}:

$$\tfrac{1}{2}Mv_{inc}^2 = E = 25.6 \text{ MeV or } 1.6 \text{ MeV/amu}$$

$$\frac{\frac{1}{2}Mv_{inc}^2}{\frac{1}{2}mv_o^2} = E/R = \frac{25.6 \text{ MeV}}{13.6 \text{ eV}}$$

$$v_{inc} = v_o \left(\frac{E/R}{M/m}\right)^{1/2} = 8v_o = 8 \text{ a.u.}$$

Calculation of cross section.

$$Z_1 = 2,\ Z_2 = 8,\ v_{inc} = 8,\ \pi a_o^2 = 8.79 \times 10^{-17}\text{cm}^2$$

$$v_{inc}/Z_2 = 8/8$$

$$\sigma(Z_1, Z_2, v_{inc}) = \frac{Z_1^2}{Z_2^4}\,\sigma(1, 1, v_{inc}/Z_2)$$

$$= \frac{4}{4096}\,\sigma(1, 1, 8/8) = \frac{1}{1024}\,2.43(\pi a_o^2)$$

$$= 2.09 \times 10^{-19}\text{cm}^2$$

For systems with 2 K-shell electrons, the results are doubled.

Table A-1

PWBA Ionization Cross Sections for p + H(1s) → p + p + e

Projectile velocity (a.u.)	Projectile energy (eV/amu)	Cross section (πa_o^2)
.05	6.248D 01	4.28D-07
.05125	6.565D 01	5.20D-07
.0525	6.888D 01	6.28D-07
.055	7.560D 01	9.06D-07
.0575	8.263D 01	1.28D-06
.06	8.997D 01	1.79D-06
.0625	9.762D 01	2.47D-06
.065	1.056D 02	3.35D-06
.0675	1.139D 02	4.50D-06
.07	1.225D 02	5.97D-06
.0725	1.314D 02	7.83D-06
.075	1.406D 02	1.02D-05
.0775	1.501D 02	1.31D-05
.08	1.599D 02	1.67D-05
.0825	1.701D 02	2.12D-05
.085	1.806D 02	2.67D-05
.0875	1.913D 02	3.32D-05
.09	2.024D 02	4.12D-05
.0925	2.138D 02	5.08D-05
.095	2.255D 02	6.22D-05
.0975	2.376D 02	7.57D-05
.1	2.499D 02	9.16D-05
.11	3.024D 02	1.87D-04
.12	3.599D 02	3.56D-04
.13	4.223D 02	6.38D-04
.14	4.898D 02	1.09D-03
.15	5.623D 02	1.77D-03
.16	6.398D 02	2.78D-03
.17	7.222D 02	4.20D-03
.18	8.097D 02	6.16D-03
.19	9.022D 02	8.80D-03

Projectile velocity (a.u.)	Projectile energy (eV/amu)	Cross section (πa_o^2)
.20	9.996D 02	1.23D-02
.225	1.265D 03	2.55D-02
.25	1.562D 03	4.75D-02
.275	1.888D 03	8.04D-02
.3	2.249D 03	1.27D-01
.35	3.061D 03	2.63D-01
.4	3.999D 03	4.57D-01
.45	5.061D 03	6.95D-01
.5	6.248D 03	9.58D-01
.55	7.560D 03	1.23D
.6	8.997D 03	1.49D
.65	1.056D 04	1.72D
.7	1.225D 04	1.92D
.75	1.406D 04	2.09D
.8	1.599D 04	2.22D
.85	1.806D 04	2.32D
.9	2.024D 04	2.38D
.95	2.255D 04	2.42D
1.	2.499D 04	2.43D
1.25	3.905D 04	2.27D
1.5	5.623D 04	1.95D
1.75	7.653D 04	1.63D
2.	9.996D 04	1.35D
2.5	1.562D 05	9.35D-01
3.	2.249D 05	6.73D-01
3.5	3.061D 05	5.05D-01
4.	3.999D 05	3.90D-01
5.	6.248D 05	2.56D-01
6.	8.997D 05	1.79D-01
7.	1.225D 06	1.31D-01
8.	1.599D 06	1.00D-01

Projectile velocity (a.u.)	Projectile energy (eV/amu)	Cross section (πa_o^2)
9.	2.024D 06	7.86D-02
10.	2.499D 06	6.29D-02
12.5	3.905D 06	3.78D-02
15.	5.623D 06	2.39D-02
17.5	7.653D 06	1.56D-02
20.	9.996D 06	1.03D-02
22.5	1.265D 07	7.03D-03
25.	1.562D 07	4.81D-03
27.5	1.890D 07	3.37D-03
30.	2.249D 07	2.41D-03
32.5	2.639D 07	1.73D-03
35.	3.061D 07	1.29D-03

SINGLE ELECTRON TRANSFER CROSS SECTIONS FOR CARBON, NITROGEN, OXYGEN, AND FLUORINE IONS INCIDENT ON HELIUM

by

THOMAS RANDALL DILLINGHAM

B. S., University of Southern Colorado, 1977

AN ABSTRACT OF A MASTER'S THESIS

submitted in partial fulfillment of the

requirement for the degree

MASTER OF SCIENCE

Department of Physics

KANSAS STATE UNIVERSITY
Manhattan, Kansas

1980

ABSTRACT

Experimentally measured single electron transfer cross sections are presented for bare nuclei and one-electron ions of carbon, nitrogen, oxygen, and fluorine following collisions with a helium gas target. The cross sections were measured as a function of projectile energy by the "initial growth method" in the range from ∿0.5 - 2.5 MeV/amu. A comparison is made between the ionization cross sections and a theoretical PWBA calculation. The agreement between experiment and theory, without inclusion of Coulomb deflection and binding energy corrections in the PWBA, is excellent, within the experimental error. Comparisons are also made between the capture cross sections and previously measured total projectile x-ray cross sections. The results confirm the magnitude of the x-ray cross sections to an accuracy of ∿30%. The ratio of the x-ray cross sections to the total capture cross section is compared to the same ratio found through a Brinkman-Kramers calculation. The results of this comparison show that the single normalization constant for the capture to each state, which was used in the theoretical analysis of the x-ray cross sections, is inadequate. In particular, the results show that the Brinkman-Kramers calculation underestimates the capture of the electron to the 1s and 2s states as compared to the higher, x-ray emitting states.